iScience

CellPress
OPEN ACCESS

Article

Biosynthesis of Circular RNA ciRS-7/CDR1as Is Mediated by Mammalian-wide Interspersed Repeats

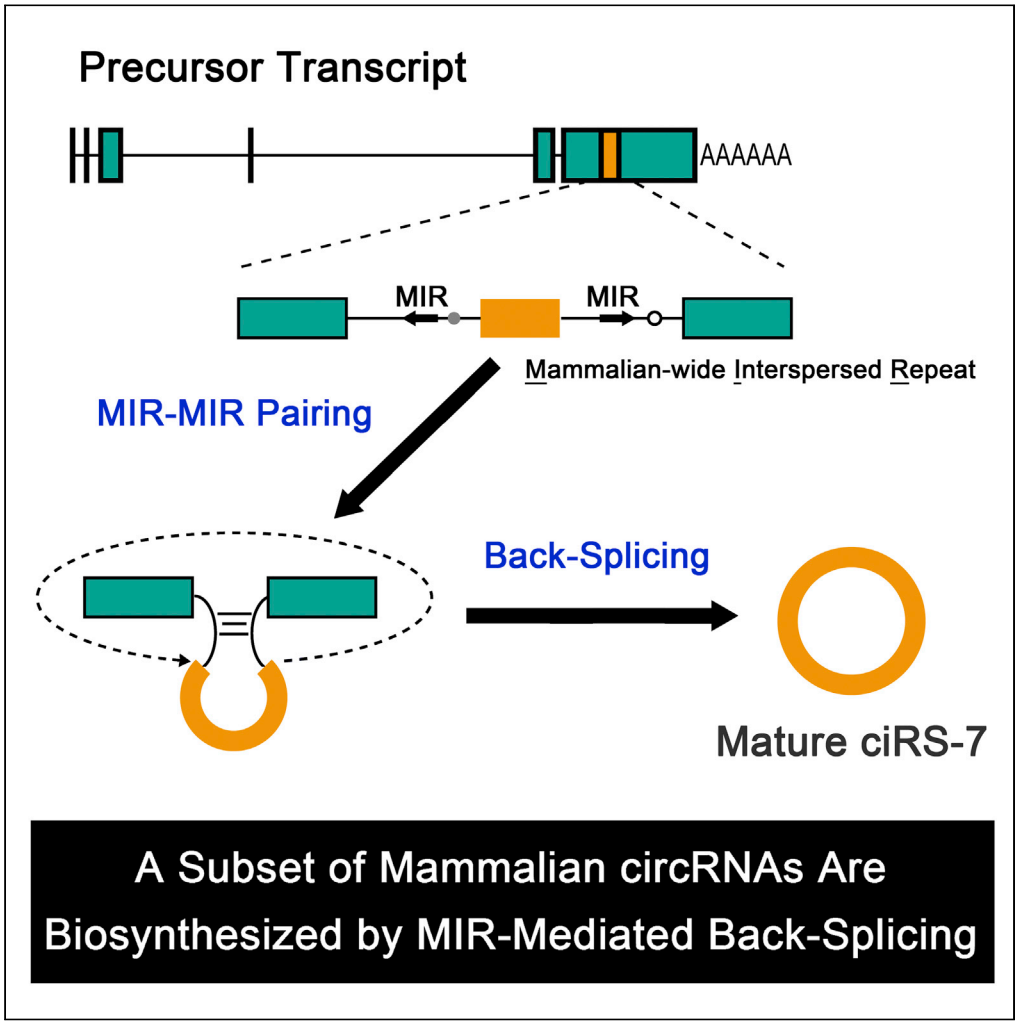

Rei Yoshimoto, Karim Rahimi, Thomas B. Hansen, Jørgen Kjems, Akila Mayeda

rei.yoshimoto@setsunan.ac.jp (R.Y.)
mayeda@fujita-hu.ac.jp (A.M.)

HIGHLIGHTS

The circular RNA, ciRS-7 (CDR1as), functions as a regulator of miR-7

ciRS-7 is generated by back-splicing, not via intra-lariat splicing

Back-splicing of ciRS-7 is promoted by the flanking inverted MIR elements

The biosynthesis of a subset of mammalian circRNAs could be mediated by MIRs

Yoshimoto et al., iScience *23*, 101345
July 24, 2020
https://doi.org/10.1016/j.isci.2020.101345

iScience

CellPress
OPEN ACCESS

Article

Biosynthesis of Circular RNA ciRS-7/CDR1as Is Mediated by Mammalian-wide Interspersed Repeats

Rei Yoshimoto,[1,4,*] Karim Rahimi,[2,3] Thomas B. Hansen,[2] Jørgen Kjems,[2,3] and Akila Mayeda[1,5,*]

SUMMARY

Circular RNAs (circRNAs) are stable non-coding RNAs with a closed circular structure. One of the best studied circRNAs is ciRS-7 (CDR1as), which acts as a regulator of the microRNA miR-7; however, its biosynthetic pathway has remained an enigma. Here we delineate the biosynthetic pathway of ciRS-7. The back-splicing events that form circRNAs are often facilitated by flanking inverted repeats of the primate-specific *Alu* elements. The ciRS-7 gene lacks these elements, but, instead, we identified a set of flanking inverted elements belonging to the mammalian-wide interspersed repeat (MIR) family. Splicing reporter assays in HEK293 cells demonstrated that these inverted MIRs are required to generate ciRS-7 through back-splicing, and CRISPR/Cas9-mediated deletions confirmed the requirement of the endogenous MIR elements in SH-SY5Y cells. Using bioinformatic searches, we identified several other MIR-dependent circRNAs and confirmed them experimentally. We propose that MIR-mediated RNA circularization is used to generate a subset of mammalian circRNAs.

INTRODUCTION

Endogenous circular RNAs (circRNAs) were first observed as scrambled exon transcripts (Nigro et al., 1991), and these transcripts were found to have circular structures with covalently closed ends (Capel et al., 1993; Cocquerelle et al., 1993). For two decades, however, they were disregarded as rare oddities, or regarded as poorly expressed mis-spliced products.

High-throughput sequencing of full transcriptomes (RNA sequencing; RNA-seq) has identified thousands of circRNAs in eukaryotes, and these are now considered common by-products of many protein-coding genes (Salzman et al., 2012; Jeck et al., 2013; Memczak et al., 2013). The significance of the vast majority of circRNAs remains unknown; however, some circRNAs have important biological functions. For instance, certain circRNAs control the stability and activity of micro RNAs (miRNAs), regulate transcription or alternative splicing, affect translation of host genes, or can even be translated and produce proteins themselves (reviewed in Wilusz, 2018). ciRS-7 (also known as CDR1as) was one of the first functionally annotated circular RNAs. It is conserved among mammals and is mainly expressed in the brain. ciRS-7 has many binding sites for a particular miRNA, miR-7, and a single binding site for miR-671 that triggers Argonaute2-catalyzed slicing of ciRS-7 (Hansen et al., 2011). *In cellulo* experiments suggested that ciRS-7 may function as a sponge, or decoy, that reduces the available free miR-7 and thus prevents repression of miR-7 targeted mRNAs (Hansen et al., 2013; Memczak et al., 2013). Knockout mice lacking the ciRS-7 genomic locus down-regulated miR-7 in the brain, suggesting that ciRS-7 has a role in stabilizing or transporting miR-7 (Piwecka et al., 2017). As a result, the ciRS-7 knockout mice had impaired sensorimotor gating, which is associated with neuropsychiatric disorders.

Recent gene editing experiments revealed a comprehensive regulatory network in mouse brain between a long non-coding RNA (lncRNA), circRNA, and two miRNAs (Kleaveland et al., 2018). This network involves the Cyrano lncRNA that promotes the degradation of miR-7, which in turn enhances the miR-671-directed degradation of ciRS-7, meaning that Cyrano causes an accumulation of ciRS-7. ciRS-7 is apparently a key component in a gene-regulatory network in the brain, but understanding the biosynthesis and transport of this particular circRNA remains an important challenge.

[1]Division of Gene Expression Mechanism, Institute for Comprehensive Medical Science, Fujita Health University, Toyoake, Aichi 470-1192, Japan

[2]Department of Molecular Biology and Genetics, Aarhus University, C.F. Møllers Allé 3, 8000 Aarhus C, Denmark

[3]Interdisciplinary Nanoscience Center, Aarhus University, Gustav Wieds Vej 14, 8000 Aarhus C, Denmark

[4]Present address: Department of Applied Biological Sciences, Faculty of Agriculture, Setsunan University, Hirakata, Osaka 573-0101, Japan

[5]Lead Contact

*Correspondence: rei.yoshimoto@setsunan.ac.jp (R.Y.), mayeda@fujita-hu.ac.jp (A.M.)

https://doi.org/10.1016/j.isci.2020.101345

It is particularly important to understand the biosynthesis of endogenous ciRS-7. In an artificial ciRS-7 expression vector, the insertion of 800 nucleotides (nt) of perfectly complementary sequences into flanking introns is technically sufficient to circularize ciRS-7 (Hansen et al., 2013); however there are no such extensive stretches of complementarity found near the endogenous ciRS-7 exon. In human, the pairing of inverted *Alu* repeats, a primate-specific repetitive element, has been shown to promote direct back-splicing in a subgroup of circRNAs (Jeck et al., 2013; Liang and Wilusz, 2014; Zhang et al., 2014; Venø et al., 2015; Zheng et al., 2016). Here we showed that highly conserved mammalian-wide interspersed repeat (MIR) sequences, but not *Alu* sequences, in the flanking introns of the ciRS-7 are required for back-splicing to generate the circular RNA structure. Bioinformatics analyses followed by reporter assays furthermore identified additional distinct circRNAs generated by inverted MIR sequences. Here, we demonstrate that a subset of mammalian circRNAs are generated by mammalian-wide MIR-mediated back-splicing.

RESULTS

Experimental Evidence Supports ciRS-7 Generation through Back-Splicing

Two major circRNA biosynthetic pathways, "Intra-lariat splicing pathway" and "Back-splicing pathway," have been proposed (Figure S1A; reviewed in Jeck and Sharpless, 2014; Wilusz, 2018). Both pathways involve a splicing reaction between downstream 5′ and upstream 3′ splice sites of the circularized exon(s); however, this splicing event occurs either directly on the loop structure formed via the flanking intronic complementary sequences in a Back-splicing pathway, or on the lariat-structure generated by exon-skipping splicing in an Intra-lariat splicing pathway (Figure S1A).

To determine the pathway used to generate ciRS-7, we first examined the ciRS-7 precursor transcript (~80 kb) that includes six non-coding exons and five introns (Figure S2). The last exon contains the entire ciRS-7 sequence, and we identified new flanking alternative 5′ and 3′ splice sites (Figures S1C and S2). We could detect closed circular form of ciRS-7 (C) together with several linear spliced products (M) due to multiple alternative 5′ and 3′ splice sites (Figure S1B). The precursor transcript (P) was also detected, and this could overlap either the lariat precursor (L1) from Intra-lariat splicing pathway or the looped form of precursor (P′) from Back-splicing pathway (Figures S1A and S1B).

The two possible pathways can be distinguished by blocking of specific splicing events using antisense oligoribonucleotides (ASOs). The ASOs 1 + 2 targeting the flanking 5′ and 3′ splice sites of ciRS-7 exon (Figures S1A and S1C; blue bars) can prevent circular ciRS-7 generation via both pathways and thus serve as the positive control (Figure S1A). In contrast, the ASOs 3–6 targeting alternative 5′ and 3′ splice sites outside of ciRS-7 exon (red bars) can prevent the exon-skipping and the following circular ciRS-7 generation in the Intra-lariat pathway (Figure S1A; left panel). However, in the Back-splicing pathway, these same ASOs 3–6 cannot interfere with the back-splicing event and would therefore allow circular ciRS-7 generation (Figure S1A; right panel). We found that ASOs 1 + 2 significantly repressed ciRS-7 production (given the efficiencies of transfection and annealing of ASOs), whereas none of the ASOs 3–6 inhibited ciRS-7 production (Figure S1D). These data thus imply that the Back-splicing pathway but not Intra-lariat pathway produces circular ciRS-7 (Figure S1A).

To further validate this finding, we made a genomic deletion of the same relevant splice sites by CRISPR-Cas9-mediated technology (Figures S3A and S3B). The deletion of either the alternative 5′ splice sites (between gRNA2 and gRNA3) or the 3′ splice sites (between gRNA4 and gRNA5) outside of ciRS-7 exon barely prevented the generation of ciRS-7 (Figure S3C), confirming that circular ciRS-7 is biosynthesized through the Back-splicing pathway but not through the Intra-lariat pathway.

The ciRS-7 Locus Is Flanked by Inverted MIR Sequences

Since our results demonstrated that the Back-splicing pathway but not the Intra-lariat splicing pathway is responsible for generating ciRS-7, we first searched for the inverted *Alu* elements thought to be required for the Back-splicing pathway. Using the UCSC RepeatMasker (in human hg19 coordinates) we identified two human *Alu* elements upstream of ciRS-7 within exon 5 and exon 6 (Figure S4) but found no downstream *Alu* element that could generate the required base pairing around the ciRS-7 exon. Therefore, flanking inverted *Alu* elements are unlikely to account for the generation of ciRS-7.

However, we did find two relatively conserved regions upstream and downstream of the ciRS-7 exon in an inverted orientation that are conserved both in human and mouse (Figure 1A). These regions overlapped

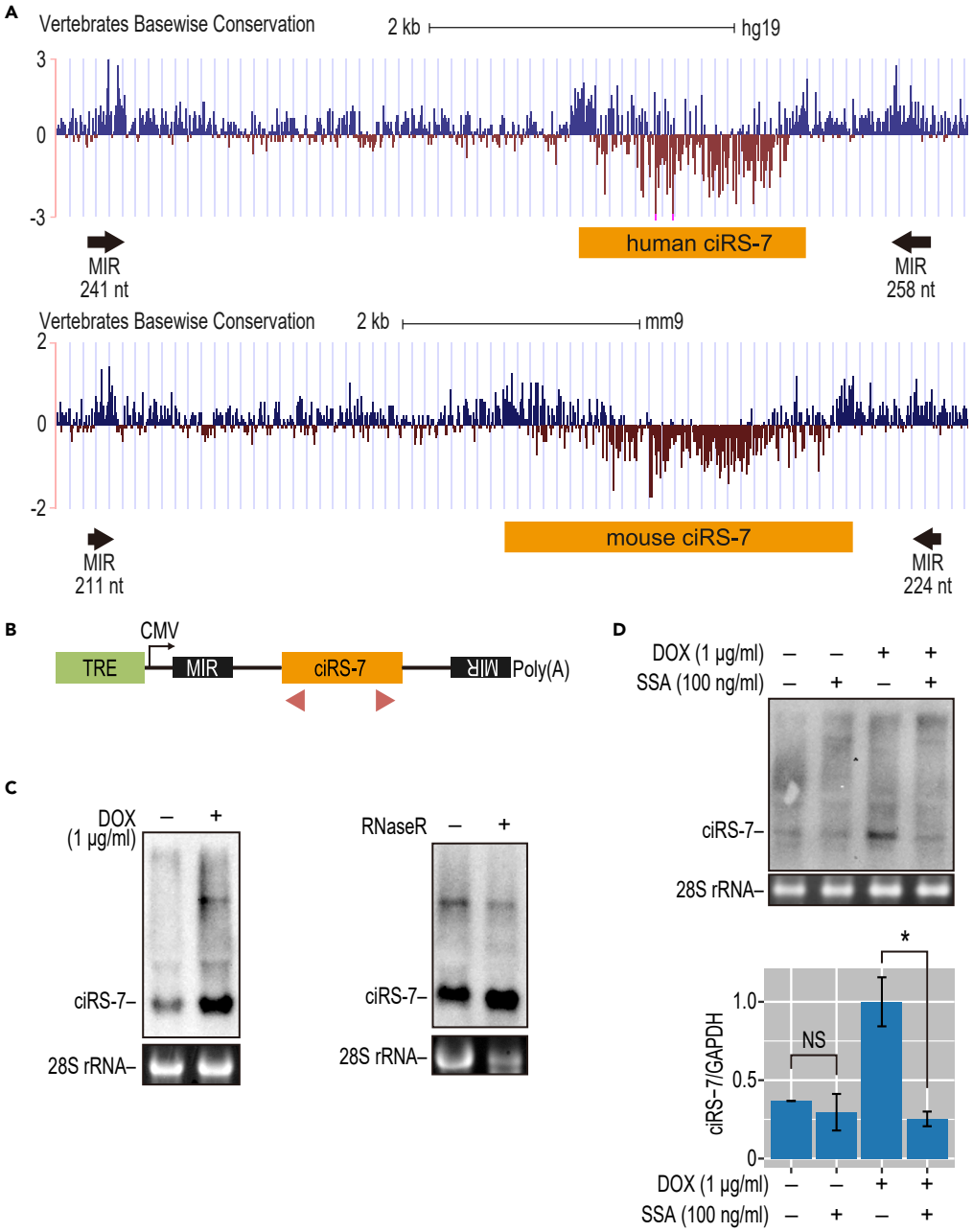

Figure 1. The Production of ciRS-7 Depends on Inverted MIRs in the Flanking Regions

(A) The ciRS-7 locus (human/mouse ciRS-7) and the identified conserved inverted MIR elements (MIRs with the lengths are indicated). The complementarity of these inverted MIRs was modeled in Figure S8. The vertebrate base-wise conservations of human (upper) and mouse (lower) genomic sequences around the ciRS-7 precursor are displayed in the UCSC Genome Browser (GRCh37/hg19 version).

(B) Schematic structure of ciRS-7-expression plasmids. Transcription is driven by a CMV promoter, and an arrow denotes the initiation site. The tetracycline response element (TRE), inverted MIR elements, ciRS-7 coding exon (ciRS-7) are indicated. Red triangle indicates the positions of PCR primers used to detect ciRS-7 and its precursor, respectively.

(C) Detection of ciRS-7 from expression plasmid in stably transduced HEK293 cells. The cells were treated with DOX and extracted total RNA was analyzed by Northern blotting (left panel). 28S rRNA was visualized by ethidium bromide staining as a loading control. To validate the circular structure of ciRS-7, total RNA was treated with RNase R prior to the Northern blotting analysis (right panel).

(D) The effect of splicing inhibitor, SSA, on the production of ciRS-7. The same stably transduced cells described in (C) were treated with DOX (+lanes) followed by SSA addition (+lanes). After 12 h culture, extracted total RNA was analyzed by

Figure 1. *Continued*
Northern blotting to detect ciRS-7 (upper panel). Ethidium bromide-stained 28S rRNA was shown as a loading control. The total RNA was also analyzed by RT-qPCR, and the graph shows quantification of the ciRS-7 generation (lower panel). ciRS-7 expression was normalized to GAPDH (ciRS-7/GAPDH) and plotted as ratios to the value of DOX-induced cells. Means ± SD are given for three independent experiments (*$p < 0.05$, NS = not significant).

with MIRs, an ancient short interspersed nuclear elements (SINE) family conserved among mammals and marsupials (Jurka et al., 1995; Krull et al., 2007). We found significant complementarities in these inverted pairs of MIRs (analyzed later), suggesting that ciRS-7 could be generated via a back-splicing pathway facilitated by inverted MIRs.

Inverted MIRs Promote ciRS-7 Biosynthesis

To test this hypothesis, we generated a stable HEK293 cell line that expresses a doxycycline (DOX)-inducible 5-kb transcript containing the ciRS-7 exon flanked by upstream and downstream inverted MIRs (Figure 1B).

The ciRS-7 circular product and its precursor RNA were both detected by Northern blot 24 h after induction with DOX (Figure 1C, left panel). We verified that the final ciRS-7 product was indeed circular by pre-treatment with RNase R (Figure 1C, right panel). These results demonstrate that our mini-gene, covering the ciRS-7 exon and its inverted MIRs, recapitulates the endogenous generation of circular ciRS-7. To test if ciRS-7 generation from the mini-gene system is splicing dependent, we used the general pre-mRNA splicing inhibitor Spliceostatin A (SSA) (Kaida et al., 2007; Yoshimoto et al., 2017). SSA clearly inhibited DOX-induced ectopic ciRS-7 production, suggesting that ciRS-7 is indeed generated by splicing (+DOX lanes, Figure 1D).

Using this stable cell line system, we next made a series of MIR-deleted mini-genes to analyze the role of MIRs in human ciRS-7 biosynthesis (Figure 2A). The wild-type mini-gene efficiently generated ciRS-7 (Figure 2B; WT), whereas the deletion of either the upstream or downstream MIR element (Δ5′MIR, Δ3′MIR, Δ5′3′MIR) and the reversion of the upstream MIR element to the same orientation as the downstream MIR element (5′MIR-RC) seriously impaired ciRS-7 production (Figures 2B and S5), demonstrating that ciRS-7 generation depends on both inverted MIRs.

Finally, we used CRISPR-Cas9-mediated editing to delete the endogenous MIR sequences in the neuronal SH-SY5Y cell line. Two guide RNAs (gRNAs) sets were designed to target the boundaries of the 5′ and 3′ MIR sequences (Figure 2C) and co-transfected with the Cas9 expression vector to delete the MIRs. The efficiencies of targeted genomic deletion were determined by PCR analyses using primers flanking the targeted regions and the PCR-amplified fragments were resolved by gel electrophoresis (Figure 2D). We observed that circularization was markedly inhibited when either the upstream or downstream MIR sequence was deleted (Figure 2E). Together, we conclude that the ciRS-7 is generated via the back-splicing pathway promoted mainly by its flanking inverted MIR sequences.

Other MIR-Dependent and MIR-Independent circRNAs Were Identified

Since MIRs are ancient SINEs and ubiquitous in mammalian genomes (Jurka et al., 1995), we speculated that the utilization of MIRs in promoting back-splicing to generate "MIR-dependent" circRNAs could be a globally conserved strategy rather than a gene-specific event.

Upon bioinformatics analysis, we indeed found that MIRs neighboring ciRS-7 are conserved among Primates, Euarchontoglires, Laurasiatheria, Afrotheria, and Armadillo. Here, we show the maps of ciRS-7 with the MIRs of human and mouse (Figure 1A). We went on to search for other potential MIR-dependent circRNAs. Using the RepeatMasker track in human hg19 coordinates, we found a total of 595,094 MIRs. Comparing with the mouse mm9 coordinates, 104,074 are conserved between human and mouse. Previously, 7,771 circRNAs were identified from RNA-seq data of foreskin cells (Jeck et al., 2013). Using this dataset, we identified 846 circRNA candidates with conserved inverted intronic MIRs within 3,000 nt upstream and downstream of the circularized exons.

From these 846 circRNA candidates, we first eliminated circRNAs with very large precursors (>5 kb) since these are hard to validate using mini-gene reporters. Among the circRNAs showing ubiquitous expression,

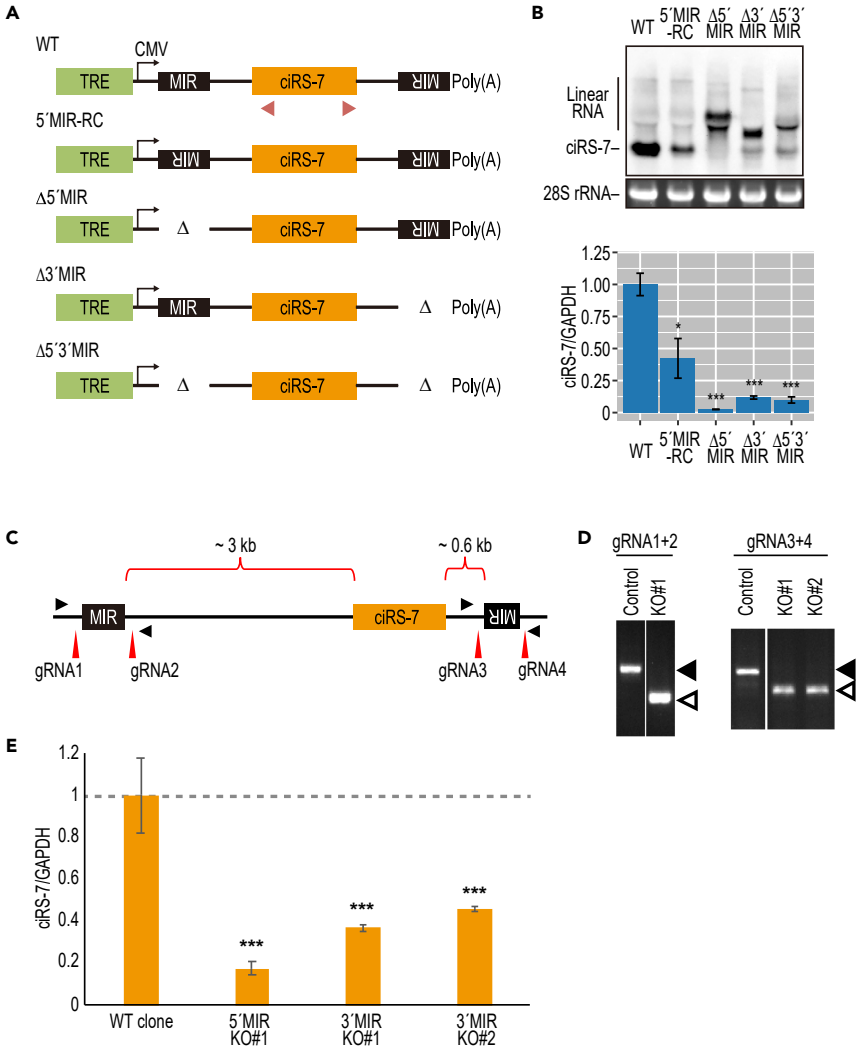

Figure 2. Deletion of Either Upstream or Downstream MIRs Diminishes the Production of ciRS-7

(A) Schematic structures of ciRS-7-expression plasmids with or without MIR sequence (see the legend of Figure 2B for CMV and TRE). Red triangles indicate the positions of PCR primers to detect ciRS-7 in (B).

(B) Generation of ciRS-7 from reporters, with or without MIR sequences, in stably transduced HEK293 cells. Total RNA extracted from the DOX-treated cells was analyzed by Northern blotting. 28S rRNA was detected by ethidium bromide staining as a control. The band corresponding to circular ciRS-7 is indicated. The upper bands observed, especially in the Δ5′/Δ3′MIR mutants, were identified as linear precursor RNAs by RNase R digestion and RT-qPCR (Figure S5). Total RNA was also quantified by RT-qPCR (lower panel). ciRS-7 expression was normalized to GAPDH (ciRS-7/GAPDH) and plotted as ratios to the value of control wild-type (WT) plasmid-expressing cells. Means ± SD are given for three independent experiments (***$p < 0.001$, *$p < 0.05$).

(C) Schematic showing the genomic structure of the ciRS-7 locus with the flanking inverted MIR sequences. The positions of guide RNAs (gRNA1–gRNA4) to delete each MIR element are indicated with red vertical arrowheads. PCR primers for detecting deleted sites are indicated with filled triangles.

(D) The genomic deletions of the flanking MIR elements in SH-SY5Y cell clones were verified by genomic PCR. The indicated two pairs of gRNAs were used to delete the 5′ and 3′ MIR elements. PCR primers indicated in (A) were used to detect the MIR deletion. Open and filled triangles point to the deleted (KO#1, KO#2) and non-deleted (Control) alleles, respectively.

(E) The effect of the homozygous MIR deletions (5′MIR KO and 3′MIR KO; #1,2 denotes cell clones in D) on ciRS-7 production was quantified by RT-qPCR. ciRS-7 expression was normalized to GAPDH in the same clones (ciRS-7/GAPDH). Values are relative to the value of control wild-type clones (WT). Means ± standard deviation (SD) are given for three independent experiments (***$p < 0.001$).

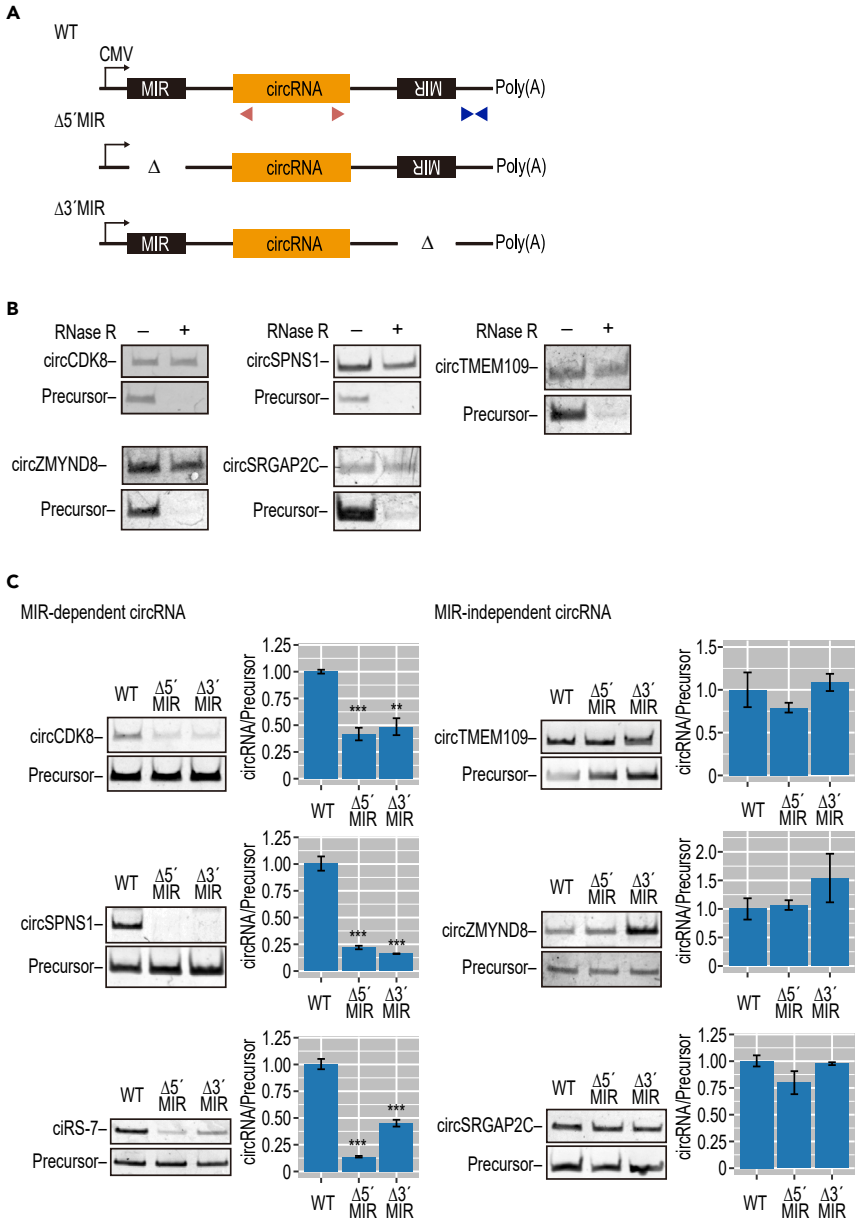

Figure 3. Several Other Human MIR-Dependent circRNAs Were Identified

(A) Schematic structure of plasmid expressing wild-type (WT) or MIR deletions (Δ5′MIR, Δ3′MIR), which was constructed for five circRNAs. Red and blue triangles indicate the positions of PCR primers to detect circRNA and precursors, respectively.

(B) RT-PCR detection of five circRNAs in mouse N2A cells transfected with the plasmids depicted in (A). Total RNA from the cells was treated with (+) or without (–) RNase R to discriminate the circular from the linear structure.

(C) Identification of MIR-dependent and MIR-independent circRNAs. RT-PCR analysis of circRNAs and their precursors, expressed from the plasmid types depicted in (A). Total RNA was also quantified by RT-qPCR. The circRNA expression levels were normalized to the expression levels of precursor RNA as controls (circRNA/Precursor). Values are relative to the value of control wild-type clones (WT). Means ± SD are given for three independent experiments (***$p < 0.001$, **$p < 0.01$).

we arbitrarily chose five circRNAs as representatives; circCDK8, circSPNS1, circTMEM109, circZYMND8, and circSRGAP2C (Figure S6 for the maps with identified MIRs). To test whether biosynthesis of these circRNAs is MIR dependent or not, we made a series of MIR-deleted mini-genes as we had done for ciRS-7 (Figure 3A). Plasmids expressing these mini-genes were transfected into mouse N2A cells, in which

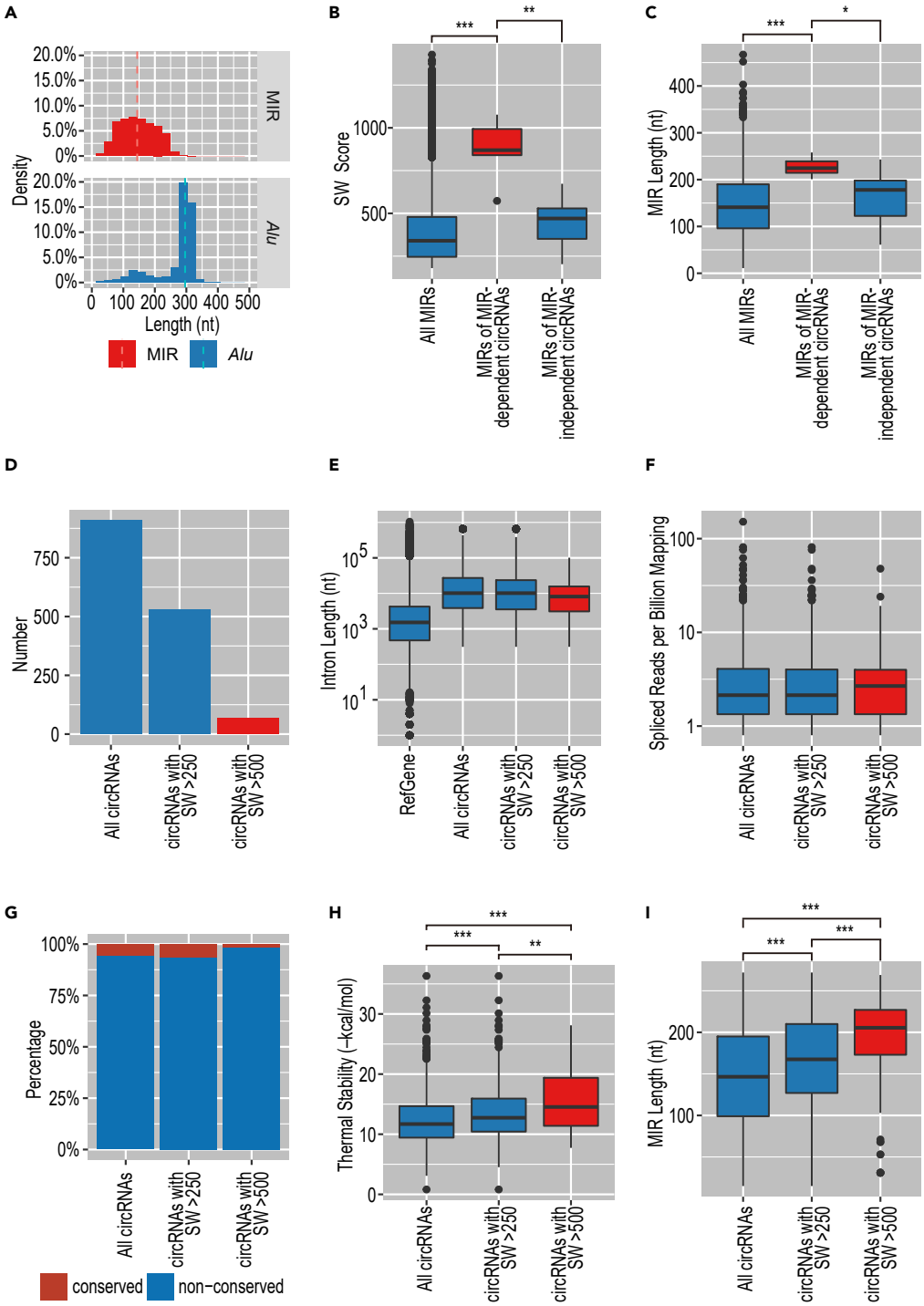

Figure 4. Biosynthesis of MIR-Dependent circRNAs Likely Depends on Stable Pairing between Highly Conserved MIRs

(A) The length distribution for MIRs is broader than for *Alus*. The bin width used in the histogram is 20 nt. A broken line indicates the median length.

(B) The verified MIR-dependent circRNAs have MIRs with near-consensus features. Boxplot of SW alignment scores of all reported MIRs, three MIR-dependent circRNAs, and three MIR-independent circRNAs (***$p < 0.001$; **$p < 0.01$). See Figure S6 for each SW score of these MIRs.

Figure 4. *Continued*

(C) The verified MIR-dependent circRNAs have longer MIRs than those of MIR-independent circRNAs. Boxplot of the MIR lengths of all reported MIRs, three MIR-dependent circRNAs, and three MIR-independent circRNAs (***$p < 0.001$; *$p < 0.05$).

(D) We identified 846 circRNAs (left bar) that have inverted MIRs within 3,000 nt of the circRNA-producing exon. Among these circRNAs, 528 circRNAs had MIRs with SW score >250 (middle bar) and 66 circRNAs had MIRs with SW score >500 (right bar).

(E) MIR-dependent circRNAs are not characterized by the flanking intron length. Boxplot shows the flanking intron lengths (nt) of the circRNAs (from the groups shown in D).

(F) MIR-dependent circRNAs are not characterized by the expression levels of circRNAs. Boxplot shows the spliced reads per billion mapping of the circRNAs (from the groups shown in D).

(G) MIR-dependent circRNAs are not characterized by the conservation rate. The orthologous circRNAs found in both human and mouse were identified as "conserved" circRNAs and the number was calculated. Bar graph shows the ratio of the conserved and non-conserved circRNAs (from the groups shown in D).

(H) MIR-dependent circRNAs are characterized by the thermal stability, suggesting that inverted MIRs with higher SW scores facilitate circularization through stable MIR-MIR pairing. Boxplot shows the thermal stabilities (–kcal/mol) of inverted MIRs of the circRNAs (from the groups shown in D), which are calculated by the RNAup program (***$p < 0.001$; **$p < 0.01$).

(I) MIR-dependent circRNAs are characterized by the relative length of the MIRs. Boxplot shows the MIR length of the circRNAs (from the groups shown in D) (***$p < 0.001$).

ectopically expressed human circRNAs could be discriminated from the endogenously expressed mouse circRNAs. All five circRNAs were successfully detected from the wild-type mini-genes, and their circular structure was verified by RNase R digestion (Figure 3B). Deletion of either upstream or downstream MIRs prevented the production of circCDK8 and circSPNS1 (Figure 3C; MIR-dependent circRNAs) but had no effect on the production of circTMEM109, circZYMND8, and circSPGAP2C (MIR-independent circRNAs).

To confirm this in an endogenous setting, CRISPR-Cas9-mediated editing was applied to delete the MIR elements flanking the circCDK8 (Figure S7A). The effective deletion was confirmed by PCR (Figure S7B). Using RT-qPCR, we observed marked inhibition of circularization when either the upstream or downstream MIR sequences were deleted (Figure S7C).

MIR-MIR Base-Pairing Stability Is Critical for circRNA Generation

MIRs are an older SINE family than *Alu*s (~130 versus ~60 million years ago), and MIR elements have often become truncated during this time (Jurka et al., 1995). In agreement with this history, the length distribution of MIRs is much broader than that for the *Alu*s (Figure 4A). We assumed that such truncations in MIRs would cause instability of the MIR-MIR base pairing required for efficient circRNA production.

To test this hypothesis, we evaluated the integrity of MIRs located around MIR-dependent and MIR-independent circRNAs by comparing them with the MIR consensus sequence using a Smith-Waterman (SW) alignment score (Smith and Waterman, 1981). As predicted, MIRs of MIR-dependent circRNAs had markedly higher alignment scores than those of MIR-independent circRNAs (Figures 4B and S6 for the individual score of all MIRs). We also observed that the MIRs of MIR-dependent circRNAs are significantly longer than those of MIR-independent circRNAs (Figure 4C).

Using these criteria of the SW alignment score, we estimated the number of MIR-dependent circRNAs from our identified 846 circRNAs with flanking inverted MIRs. We found that 528 and 66 circRNAs have higher SW scores than 250 and 500, respectively (Figure 4D). The high MIR-SW scores (573–1,077; Figures 3C and S6A and the legend) seen for the experimentally confirmed MIR-dependent circRNAs suggest that these 66 circRNAs (>500 MIR-SW scores) are all likely to be biosynthesized by an MIR-dependent pathway. Then we analyzed these two sets of circRNAs (SW > 250 and SW > 500) in relation to length of the flanking intron (Figure 4E), the expression level (Figure 4F), the conservation rate (Figure 4G), and the thermal stability of MIR-MIR pairing (Figure 4H). The comparisons demonstrate that these two sets of circRNAs (SW > 250 and SW > 500) can be well characterized by the thermal stability. Together, circRNAs with higher SW alignment scores can form more stable MIR-MIR pairing (Figure 4H), which might be attributed to the relatively long length of MIRs (Figure 4I). To validate this notion, the 5′ MIR of the ciRS-7 expressing plasmid was shortened by stepwise trimming from the 5′ end (Figure 5A) and the ciRS-7 generation was examined (Figures 5B and 5C). The ciRS-7 generation was gradually decreased from the deleted MIR length of 191 nt (51–241), 141 nt

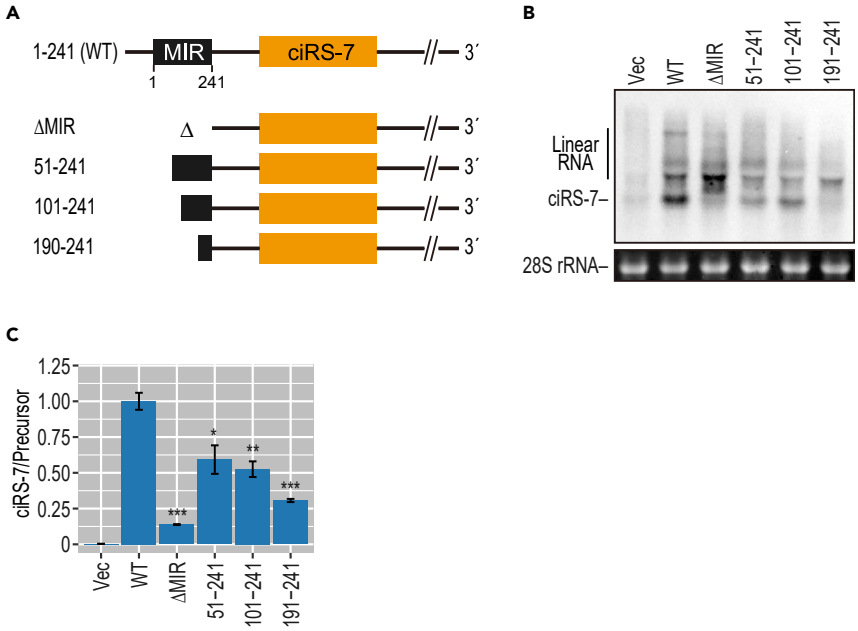

Figure 5. Shortening the Flanking MIRs Reduces circRNA Biosynthesis

(A) Schematic structures of MIR-deleted ciRS-7-expression plasmids. The numbers indicate the lengths of the deleted 5′ MIR elements.

(B) Generation of ciRS-7 from reporters, with various MIR lengths, in transiently transfected ciRS-7 knockout HEK293 cells. Total RNA extracted from DOX-treated cells was analyzed by Northern blotting. 28S rRNA was detected by ethidium bromide staining as a control. The band corresponding to ciRS-7 is indicated on the left (see Figure 2B legend for the upper products).

(C) ciRS-7 formation was also quantified by RT-qPCR. Expression levels were normalized to the level of precursor RNA (ciRS-7/Precursor) and plotted as ratios to the value of control wild-type (WT) plasmid-expressing cells. Therefore, these quantified results do not exactly match up to the apparent view of Northern data in (B). Means ± SD are given for three independent experiments (***$p < 0.001$, **$p < 0.01$, *$p < 0.05$).

(101–241), and 51 nt (190–241), indicating that the efficient back-splicing requires at least 200 nt length of the inverted MIRs, which is exactly consistent with the MIR length distribution of MIR-dependent circRNAs (Figure 4C).

The predicted complementarity of inverted MIRs of all six selected circular RNAs together with three *Alu*-dependent circRNAs revealed that the MIR-MIR base pairings of MIR-dependent circRNAs are generally more stable than those of MIR-independent circRNAs, although not so much as those of *Alu*-dependent circRNAs (Figure S8). We experimentally tested the efficiency of the flanking MIRs and *Alu*s elements in generating ciRS-7 using heterologous ciRS-7 expressing plasmids (Figure 6). Notably, the insertion of heterologous *Alu* elements (derived from circHIPK3 intron) in the ciRS-7 expression construct supported even weaker back-splicing activity compared with the original ciRS-7 construct (Figure 6), suggesting that not only the stability of base pairing but also the combination between flanking inverted sequences and the ciRS-7 exon affects in the efficiency of circularization. Together, we conclude that a subset of mammalian circRNAs contains evolutionally conserved, flanking, and inverted MIRs that mediate circularization via stable pairing.

DISCUSSION

We and others first characterized the circular RNA ciRS-7 as a regulator of a specific miRNA, miR-7 (Hansen et al., 2013; Memczak et al., 2013). Here, we describe the biosynthetic pathway for this important circRNA. Circular ciRS-7 is formed via a back-splicing process that is facilitated by flanking inverted sequences derived from MIR, a conserved mammalian SINE. Furthermore, we identified MIR-derived elements that are associated with a number of circRNAs and promote back-splicing and circularization, illustrating a distinct subset of mammalian circRNAs whose formation is driven by MIRs but not by *Alu*s.

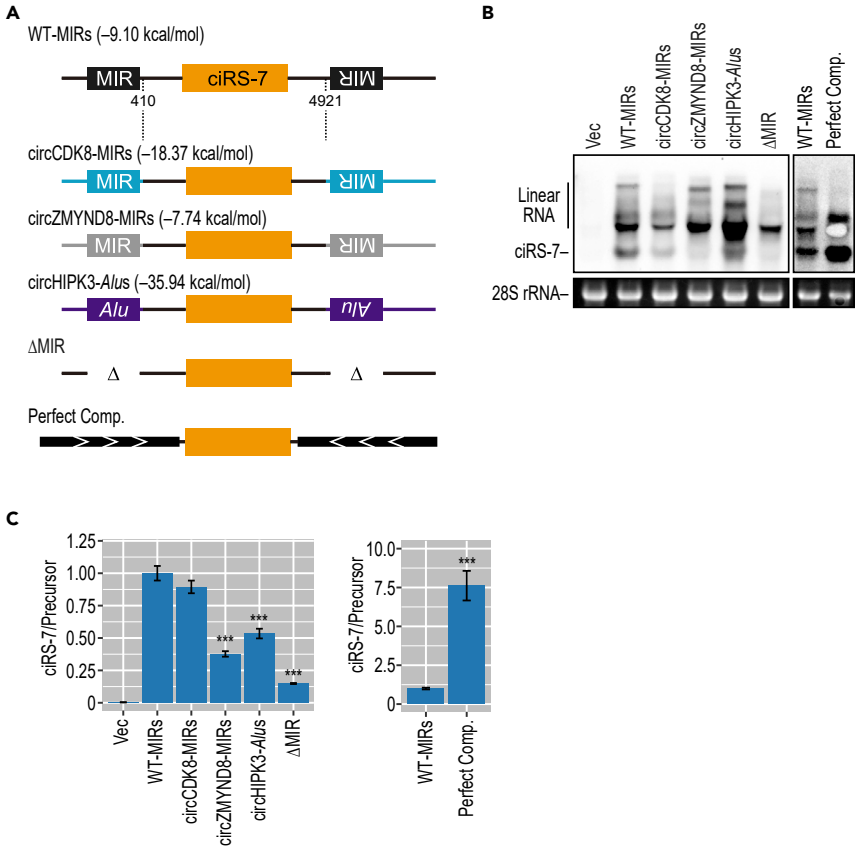

Figure 6. The Flanking Inverted Repeats and the ciRS-7 Exon Are Cooperative in ciRS-7 Circularization

(A) Schematic structures of chimeric ciRS-7-expressing reporters with heterologous flanking repeated elements. The indicated heterologous MIR and *Alu* elements were inserted in flanking introns of the ciRS-7 expressing plasmid (used in Figure 1B). The ciRS-7 expressing plasmid with ~800-nt flanking inverted elements (Hansen et al., 2013) was used for comparison.

(B) Generation of ciRS-7 from reporters, with heterologous flanking repeated elements, in transiently transfected ciRS-7 knockout HEK293 cells. Total RNA extracted from the transfected cells was analyzed by Northern blotting. 28S rRNA was detected by ethidium bromide staining as a control. Produced ciRS-7 and linear RNA are indicated on the left (see Figure 2B legend for the linear products).

(C) ciRS-7 formation was also quantified by RT-qPCR. Expression levels were normalized to the level of precursor RNA (ciRS-7/Precursor) and plotted as ratios to the value of control WT-MIRs plasmid-expressing cells. Therefore, these quantified results do not exactly match up to the apparent view of Northern data in (B). Means ± SD are given for three independent experiments (***$p < 0.001$).

Previous Results Are Consistent with the MIR-Dependent Back-Splicing of ciRS-7

Previous ciRS-7 back-splicing assays used reporter plasmids that include the endogenous flanking genomic sequence, 1 kb upstream and 0.2 kb downstream of the ciRS-7 exon (Hansen et al., 2013). This reporter could not produce ciRS-7, consistent with the fact that the inverted MIRs required for back-splicing are located ~3.0 kb and ~0.6 kb away from the 3′ and 5′ splice sites of ciRS-7 exon, respectively.

The genomic structure around the ciRS-7 precursor has been independently reported (Barrett et al., 2017). In agreement with our analysis, this study showed that the promoter region of ciRS-7 overlaps an upstream long non-coding transcript (LINC00632 locus), suggesting that the ciRS-7 precursor is a long non-coding RNA (Barrett et al., 2017). The BAC clones obtained (185 and 200 kb) cover from the promoter of this non-coding transcript (LINC00632) to far downstream of the ciRS-7 exon and they were found to produce mature ciRS-7. The rationale is that these two BAC clones include upstream and downstream MIRs that are essential for ciRS-7 generation as we showed here.

MIR-Dependent Back-Splicing Is Widely Utilized for Mammalian circRNA Biosynthesis

The direct back-splicing pathway is commonly used to generate circRNA in metazoans, and flanking inverted elements were shown to promote this event (reviewed in Wilusz, 2018). Although non-repetitive complementary sequences were reported to promote particular back-splicing events in human and fruit fly (Zhang et al., 2014; Kramer et al., 2015), *Alus* are major players in the biosynthesis of human circRNAs (Jeck et al., 2013; Zhang et al., 2014) because of their abundance (~10% in human genome; Price et al., 2004). However, the *Alu*-SINEs are relatively young elements (~60 million years) and exist only in primates. MIR-SINEs are much older (~130 million years) and globally functional in mammals (Krull et al., 2007), making it likely that MIRs are commonly used in the biosynthesis of mammalian circRNAs.

Owing to their age, many MIR sequences have lost their 5′ and 3′ regions, reducing their potential to form complementary duplexes, whereas the more recently emerged *Alu* sequences have remained more complementary to one another. An earlier study found that short complementary sequences (30–40 nt) in the inverted *Alu* elements are required to support efficient back-splicing (Liang and Wilusz, 2014). According to this criterion, the MIR-independent circRNAs may not have to possess complementary sequences longer than 30 nt. Notably, the difference between MIR-dependent and MIR-independent circRNAs was reflected in the predicted secondary structures of their MIR sequences (Figure S8). We assume that other types of flanking complementary elements with the possible aid of RNA-protein interactions may explain the formation of these MIR-independent circRNAs (reviewed in Wilusz, 2018).

In human, it is possible that the MIR-dependent circRNAs are also flanked by more stable inverted *Alu* elements. Indeed, we found that 24 of all 66 MIR-dependent circRNAs (including circCDK8) are flanked by inverted *Alu* elements. Nevertheless, the CRISPR-Cas9-mediated deletion of only either the 5′ or 3′ MIR element was sufficient to prevent its circularization. We assume that inverted *Alu*-*Alu* pairing within either upstream or downstream flanking introns could prevent inverted *Alu*-dependent back-splicing as reported previously (Zhang et al., 2014) and we found that is exactly the case in 12 MIR-dependent circRNAs.

MIR Deletion Could Be an Effective Way to Investigate Function of Targeted circRNA

Our bioinformatics analysis identified 66 circRNAs with conserved flanking MIRs with high complementarity (SW score >500), and these are thus expected to be formed via an MIR-dependent pathway. As the representative of these, we verified that circCDK8 and circSPNS1, as well as ciRS-7, were indeed generated through flanking inverted MIR elements.

The host genes of these MIR-dependent circRNAs, circCDK8 and circSPNS1, have important biological roles. CDK8 kinase is a component of the Mediator kinase complex that regulates transcription by RNA Polymerase II (reviewed in Dannappel et al., 2019). The SPNS1 protein is a putative lysosomal H^+-carbohydrate transporter that is required for autophagy (Sasaki et al., 2014; Sasaki et al., 2017; and references therein). Since exon circularization via back-splicing and linear mRNA production via authentic splicing from the same pre-mRNA are mutually exclusive events in back-splicing pathway (see Figure S1A), circRNA formation could potentially regulate the expression of the host gene (Ashwal-Fluss et al., 2014; reviewed in Wilusz, 2018).

To examine the unknown functions of these MIR-derived circRNAs, it is essential to knock out the target circRNA while retaining the host gene expression, or the normal spliced mRNA. Previously, it was shown that the CRISPR-Cas9-mediated deletion of an intronic complementary element successfully blocked circRNA formation without any effect on the linear mRNA splicing (Zhang et al., 2016). Therefore, we will take advantage of the detected MIRs to specifically attenuate circRNA expression using the CRISPR-Cas9 technique. Our investigation of the phenotype in the MIR-targeted knockdown cells will shed light on the biological and physiological functions of circCDK8 and circSPNS1.

Limitations of the Study

We demonstrate the biosynthetic pathway of the functionally important circRNA, ciRS-7 (CDR1as). The essential back-splicing process is facilitated by flanking inverted elements of MIR but not by those of the previously known primate-specific *Alu* repeats. Our bioinformatics analysis suggests that the MIR-dependent biosynthesis applies to a large number of circRNAs but a full experimental validation for the entire subset remains to be performed.

Resource Availability

Lead Contact

Further information and requests for resources and reagents should be directed to and will be fulfilled by the Lead Contact, Akila Mayeda (mayeda@fujita-hu.ac.jp).

Materials Availability

This study did not generate new unique reagents.

Data and Code Availability

This study did not generate/analyze datasets/code.

METHODS

All methods can be found in the accompanying Transparent Methods supplemental file.

SUPPLEMENTAL INFORMATION

Supplemental Information can be found online at https://doi.org/10.1016/j.isci.2020.101345.

ACKNOWLEDGMENTS

We are grateful to Drs. Kinji Ohno and Hitomi Tsuiji for SH-SY5Y cells and N2A cells, respectively. Spliceostatin A (SSA) was a generous gift from Dr. Minoru Yoshida. We thank Dr. Karoline Ebbesen for sharing unpublished data; Drs. Anne Nielsen, Shinichi Nakagawa, and Julian Venables for critical reading of the manuscript; Dr. Makoto K. Shimada for helpful suggestions for bioinformatics analysis; Taiwa Komatsu and Mayuko Tanahashi for providing instruction of the gene editing techniques, and members of our laboratory for constructive discussion.

R.Y. was supported by a Research Grant from the Hori Sciences and Arts Foundation, a Research Grant from the Nitto Foundation, a Science Research Promotion Fund from the Promotion and Mutual Aid Corporation for Private Schools of Japan (PMAC), and Grants-in-Aid for Scientific Research (C) (JP18K05563). A.M. was partly supported by Grants-in-Aid for Scientific Research (B) (JP16H04705) and Grants-in-Aid for Challenging Exploratory Research (JP16K14659) from the Japan Society for the Promotion of Science (JSPS). K.R. was supported by Villum Foundation.

AUTHOR CONTRIBUTIONS

R.Y. and A.M. conceived and designed the experiments; R.Y. conducted most of the experiments, organized the data, and drafted the manuscript; K.R. performed CRISPR-Cas9-mediated genomic deletion of the MIR elements; T.B.H. and J.K. provided useful information and revised the manuscript; A.M. analyzed the data and edited the manuscript. A.M. coordinated and supervised the whole project. All authors read, corrected, and approved the final paper.

DECLARATION OF INTERESTS

The authors declare no competing interests.

Received: June 26, 2019
Revised: April 18, 2020
Accepted: July 2, 2020
Published: July 24, 2020

REFERENCES

Ashwal-Fluss, R., Meyer, M., Pamudurti, N.R., Ivanov, A., Bartok, O., Hanan, M., Evantal, N., Memczak, S., Rajewsky, N., and Kadener, S. (2014). circRNA biogenesis competes with pre-mRNA splicing. Mol. Cell *56*, 55–66.

Barrett, S.P., Parker, K.R., Horn, C., Mata, M., and Salzman, J. (2017). ciRS-7 exonic sequence is embedded in a long non-coding RNA locus. PLoS Genet. *13*, e1007114.

Capel, B., Swain, A., Nicolis, S., Hacker, A., Walter, M., Koopman, P., Goodfellow, P., and Lovell-Badge, R. (1993). Circular transcripts of the testis-determining gene Sry in adult mouse testis. Cell *73*, 1019–1030.

Cocquerelle, C., Mascrez, B., Hetuin, D., and Bailleul, B. (1993). Mis-splicing yields circular RNA molecules. FASEB J. *7*, 155–160.

Dannappel, M.V., Sooraj, D., Loh, J.J., and Firestein, R. (2019). Molecular and *in vivo* functions of the CDK8 and CDK19 kinase modules. Front. Cell Dev. Biol. *6*, 171.

Hansen, T.B., Jensen, T.I., Clausen, B.H., Bramsen, J.B., Finsen, B., Damgaard, C.K., and Kjems, J. (2013). Natural RNA circles function as efficient microRNA sponges. Nature *495*, 384–388.

Hansen, T.B., Wiklund, E.D., Bramsen, J.B., Villadsen, S.B., Statham, A.L., Clark, S.J., and Kjems, J. (2011). miRNA-dependent gene silencing involving Ago2-mediated cleavage of a circular antisense RNA. EMBO J. *30*, 4414–4422.

Jeck, W.R., and Sharpless, N.E. (2014). Detecting and characterizing circular RNAs. Nat. Biotechnol. *32*, 453–461.

Jeck, W.R., Sorrentino, J.A., Wang, K., Slevin, M.K., Burd, C.E., Liu, J., Marzluff, W.F., and Sharpless, N.E. (2013). Circular RNAs are abundant, conserved, and associated with ALU repeats. RNA *19*, 141–157.

Jurka, J., Zietkiewicz, E., and Labuda, D. (1995). Ubiquitous mammalian-wide interspersed repeats (MIRs) are molecular fossils from the mesozoic era. Nucleic Acids Res. *23*, 170–175.

Kaida, D., Motoyoshi, H., Tashiro, E., Nojima, T., Hagiwara, M., Ishigami, K., Watanabe, H., Kitahara, T., Yoshida, T., Nakajima, H., et al. (2007). Spliceostatin A targets SF3b and inhibits both splicing and nuclear retention of pre–mRNA. Nat. Chem. Biol. *3*, 576–583.

Kleaveland, B., Shi, C.Y., Stefano, J., and Bartel, D.P. (2018). A network of noncoding regulatory RNAs acts in the mammalian brain. Cell *174*, 350–362.e17.

Kramer, M.C., Liang, D., Tatomer, D.C., Gold, B., March, Z.M., Cherry, S., and Wilusz, J.E. (2015). Combinatorial control of Drosophila circular RNA expression by intronic repeats, hnRNPs, and SR proteins. Genes Dev. *29*, 2168–2182.

Krull, M., Petrusma, M., Makalowski, W., Brosius, J., and Schmitz, J. (2007). Functional persistence of exonized mammalian-wide interspersed repeat elements (MIRs). Genome Res. *17*, 1139–1145.

Liang, D., and Wilusz, J.E. (2014). Short intronic repeat sequences facilitate circular RNA production. Genes Dev. *28*, 2233–2247.

Memczak, S., Jens, M., Elefsinioti, A., Torti, F., Krueger, J., Rybak, A., Maier, L., Mackowiak, S.D., Gregersen, L.H., Munschauer, M., et al. (2013). Circular RNAs are a large class of animal RNAs with regulatory potency. Nature *495*, 333–338.

Nigro, J.M., Cho, K.R., Fearon, E.R., Kern, S.E., Ruppert, J.M., Oliner, J.D., Kinzler, K.W., and Vogelstein, B. (1991). Scrambled exons. Cell *64*, 607–613.

Piwecka, M., Glazar, P., Hernandez-Miranda, L.R., Memczak, S., Wolf, S.A., Rybak-Wolf, A., Filipchyk, A., Klironomos, F., Cerda Jara, C.A., Fenske, P., et al. (2017). Loss of a mammalian circular RNA locus causes miRNA deregulation and affects brain function. Science *357*, eaam8526.

Price, A.L., Eskin, E., and Pevzner, P.A. (2004). Whole-genome analysis of Alu repeat elements reveals complex evolutionary history. Genome Res. *14*, 2245–2252.

Salzman, J., Gawad, C., Wang, P.L., Lacayo, N., and Brown, P.O. (2012). Circular RNAs are the predominant transcript isoform from hundreds of human genes in diverse cell types. PLoS One *7*, e30733.

Sasaki, T., Lian, S., Khan, A., Llop, J.R., Samuelson, A.V., Chen, W., Klionsky, D.J., and Kishi, S. (2017). Autolysosome biogenesis and developmental senescence are regulated by both Spns1 and v-ATPase. Autophagy *13*, 386–403.

Sasaki, T., Lian, S., Qi, J., Bayliss, P.E., Carr, C.E., Johnson, J.L., Guha, S., Kobler, P., Catz, S.D., Gill, M., et al. (2014). Aberrant autolysosomal regulation is linked to the induction of embryonic senescence: differential roles of Beclin 1 and p53 in vertebrate Spns1 deficiency. PLoS Genet. *10*, e1004409.

Smith, T.F., and Waterman, M.S. (1981). Identification of common molecular subsequences. J. Mol. Biol. *147*, 195–197.

Venø, M.T., Hansen, T.B., Venø, S.T., Clausen, B.H., Grebing, M., Finsen, B., Holm, I.E., and Kjems, J. (2015). Spatio-temporal regulation of circular RNA expression during porcine embryonic brain development. Genome Biol. *16*, 245.

Wilusz, J.E. (2018). A 360 degrees view of circular RNAs: from biogenesis to functions. WIREs RNA *9*, e1478.

Yoshimoto, R., Kaida, D., Furuno, M., Burroughs, A.M., Noma, S., Suzuki, H., Kawamura, Y., Hayashizaki, Y., Mayeda, A., and Yoshida, M. (2017). Global analysis of pre-mRNA subcellular localization following splicing inhibition by spliceostatin A. RNA *23*, 47–57.

Zhang, X.O., Wang, H.B., Zhang, Y., Lu, X., Chen, L.L., and Yang, L. (2014). Complementary sequence-mediated exon circularization. Cell *159*, 134–147.

Zhang, Y., Xue, W., Li, X., Zhang, J., Chen, S., Zhang, J.L., Yang, L., and Chen, L.L. (2016). The biogenesis of nascent circular RNAs. Cell Rep. *15*, 611–624.

Zheng, Q., Bao, C., Guo, W., Li, S., Chen, J., Chen, B., Luo, Y., Lyu, D., Li, Y., Shi, G., et al. (2016). Circular RNA profiling reveals an abundant circHIPK3 that regulates cell growth by sponging multiple miRNAs. Nat. Commun. *7*, 11215.

iScience, Volume *23*

Supplemental Information

Biosynthesis of Circular RNA ciRS-7/CDR1as Is Mediated by Mammalian-wide Interspersed Repeats

Rei Yoshimoto, Karim Rahimi, Thomas B. Hansen, Jørgen Kjems, and Akila Mayeda

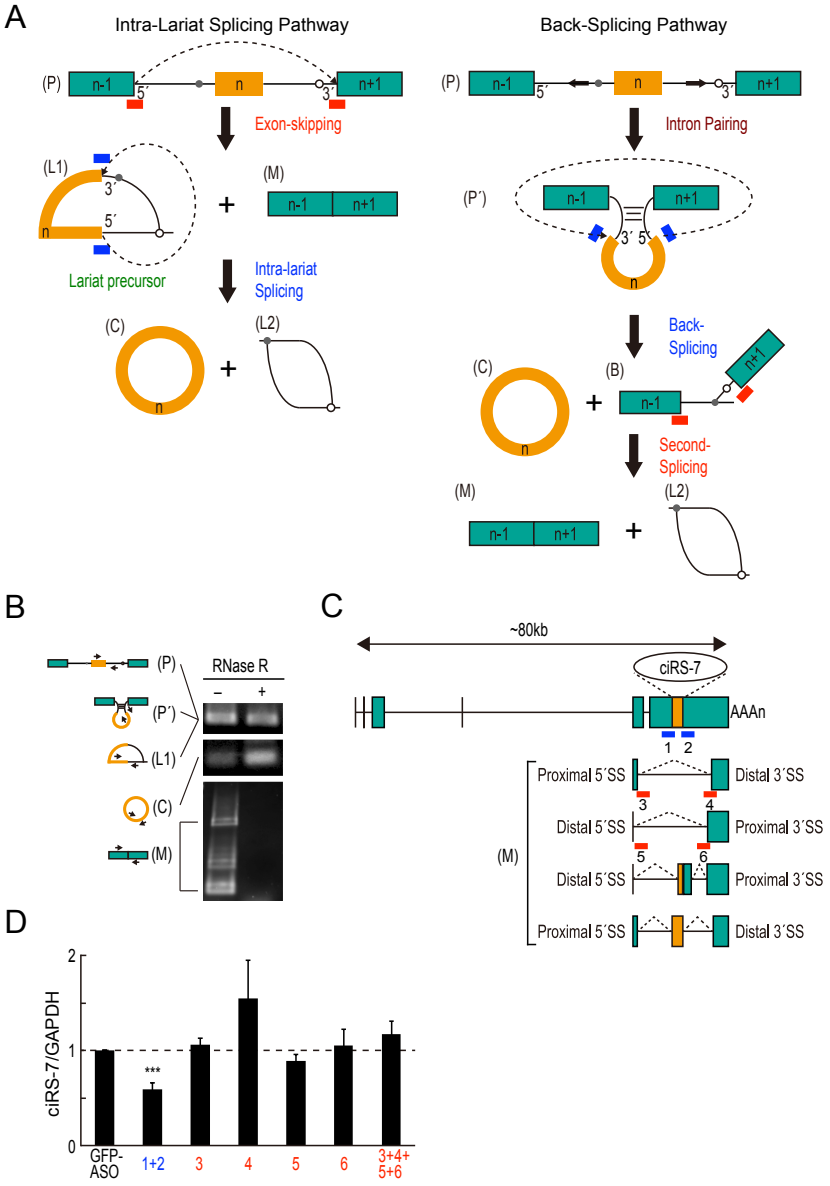

Figure S1. Evidence for 'Back-splicing' rather than 'Intra-lariat splicing' to produce circular ciRS-7
(Related to Figure 1)
(A) Two proposed pathways for circRNA biosynthesis. Left panel: the generation by an intra-lariat splicing of lariat precursor (L1) that is excised by the preceding exon(s)-skipped splicing of pre-mRNA (P). Right panel: the circRNA (C) generation by a direct back-splicing event that is promoted by the looped pre-mRNA (P′) formed by base-paring of the flanking intronic complementary sequences. Blue and red bars indicate the antisense oligoribonucleotides (ASOs), numbered 1–6 in panels C and D, annealed to prevent the following pathways (Exon-skipping, Intra-lariat splicing, Back-splicing, or Second-splicing).
(B) Detection of intermediates (P', L1) and products (C, M) from the ciRS-7 precursor (P). Total RNA from human cerebral cortex was treated with (+) or without (–) RNase R to distinguish opened linear RNA from closed RNA. The purified RNA was analyzed by RT–PCR with indicated primers (arrowheads).
(C) Schematic representation of the ciRS-7 precursor and the alternatively spliced isoforms (see panel B and Figure S2). Bars indicate ASOs (1–6) to block specific alternative splicing event.
(D) The quantified data of splicing prevention using ASOs (1–6; see panel C). SH-SY5Y cells were electroporated with each ASO. After 24 h incubation, RT–PCR analysis was performed with ciRS-7 primers and the control GAPDH primers. The detected ciRS-7 expression levels were normalized to GAPDH (ciRS-7/GAPDH) and plotted as ratios to the value of control cells treated with GFP-ASO. Means ± standard deviation (SD) are given for three independent experiments (***P < 0.001).

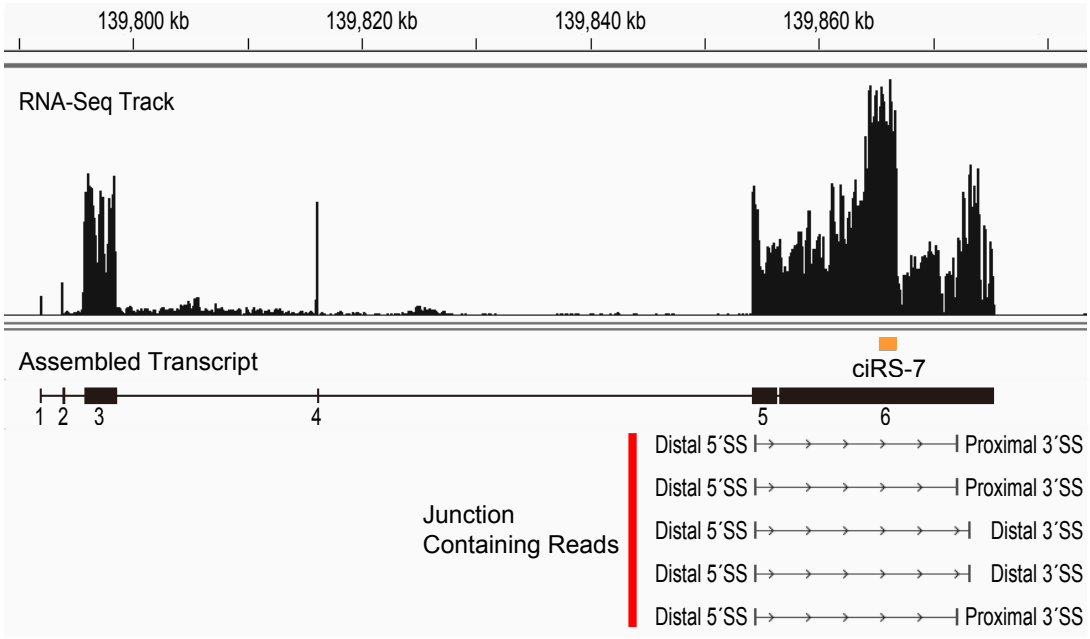

Figure S2. Identified Alternative Splice Sites Might Cause Skipping of the ciRS-7 Exon
(Related to Figures 1, S1)
Modified screeenshot of human brain RNA-Seq data (GSE59612) mapped on the the human hg19 genome sequence is indicating the assembled ciRS-7 precursor transcript. The junction containing reads revealed the active alternative 5′ and 3′ splice sites within the exons 5 and 6.

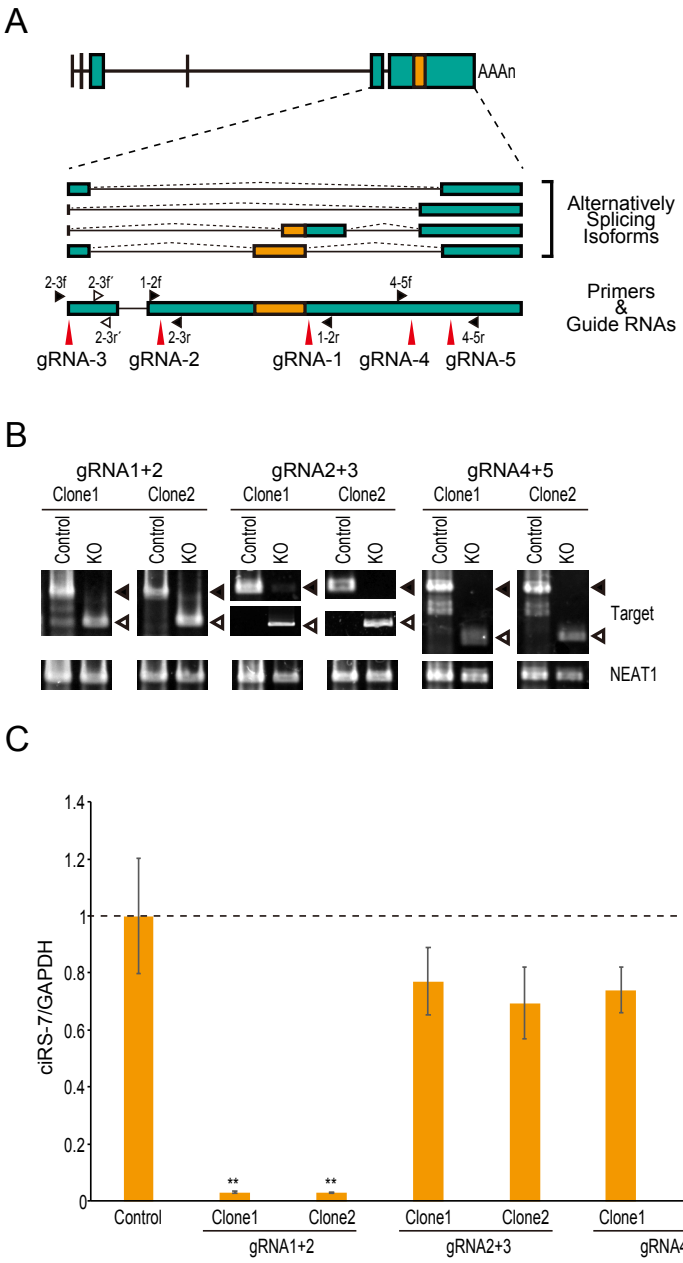

Figure S3. CRISPR/Cas9-Mediated Deletion of the Flanking Alternative Splice Sites in ciRS-7 Gene Supports 'Back-Splicing Pathway' in Biosynthesis of ciRS-7

(Related to Figures 1, S1)

(A) Schematic structures of the ciRS-7 precursor and its alternatively spliced isoforms (orange box indicates ciRS-7 exon). The positions of the guide RNAs (gRNA1–gRNA5) targetting the alternative splice sites used in 'Intra-lariat splicing pathway' (Figure S1A), PCR primers for detecting deleted sites (filled triangles), and those for detecting un-deleted sites (open triangeles) are also indicated.

(B) The targeted ciRS-7 genomic deletions in HEK-293 cells were verified by genomic PCR. The indicated three pairs of gRNAs were used to delete the alternative splice sites. PCR primers indicated in panel A were used for detecting deleted sites (open triangles) and non-deleted sites (filled triangles). PCR primers for the *NEAT1* gene were used as control.

(C) The deletion of either the alternative 5′ splice sites (between gRNA2 and gRNA3) or the 3′ splice sites (between gRNA4 and gRNA5) outside of ciRS-7 exon barely prevented the generation of ciRS-7. The ciRS-7 production was analyzed by quantitative RT–PCR with ciRS-7 primers and the control GAPDH primers. The ciRS-7 expression levels were normalized to the control expression level of GAPDH (ciRS-7/GAPDH). The results were plotted as ratios to the value of control wild-type cells. Means ± standard deviation (SD) are given for three independent experiments (**P < 0.01).

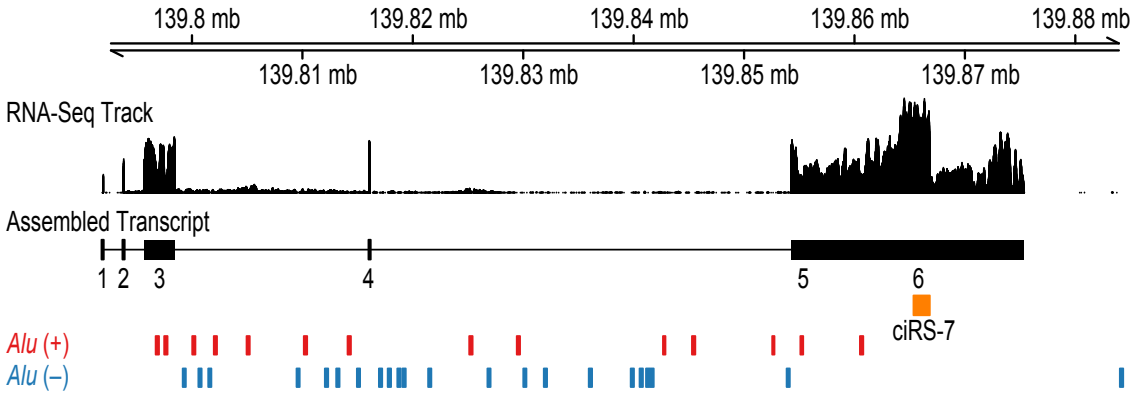

Figure S4. The ciRS-7 Exon Is Not Flanked by Inverted *Alu* Elements
(Related to Figure 1)
The locations of the human genomic *Alu* elements are shown together with the assembled ciRS-7 precursor transcript (see Figure S2 above). The *Alu* elements (bars) were extracted from UCSC Repeat Masker database (+ and – are the same and opposite strand of the ciRS-7 exon, respectively). Analysis of 3′ rapid amplification of cDNA ends (RACE) detected the 3′ terminal of ciRS-7 precursor with canonical poly (A) tail (from downstream of chrX: 139873517), indicating that the transcript is terminated around the end of exon 6.

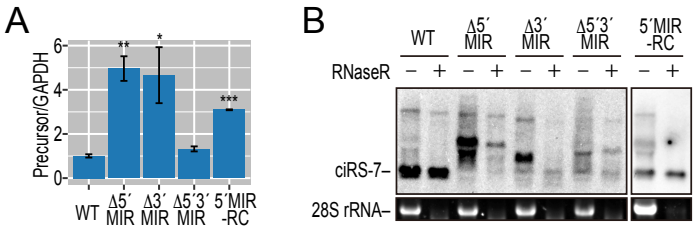

Figure S5. Deletion of Flanking MIRs Causes Accumulation of Precursor
(Related to Figure 2)
(A) Total RNA (used in Figure 2B) was quantified by RT–qPCR. The ciRS-7 precursor expression levels were normalized to GAPDH (Precursor/GAPDH) and compared to wild-type (WT) plasmid-expressing HEK293 cells. Means ± SD are given for three independent experiments. Means ± SD are given for three independent experiments (***P < 0.001, **P < 0.01, *P < 0.05).
(B) Total RNA (used in Figure 2B), with (+) or without (–) RNase R treatment, was analyzed by Northern blotting.

Figure S6. Additional Human circRNAs Were Identifed with Flanking Inverted MIR Elements
(Related to Figure 3)
The loci of two MIR-dependent circRNAs **(A)** and three MIR-independent circRNAs **(B)** are shown. The positions of the host genes (with red numbered exons), circRNA exons (orange boxes), and the identified inverted MIR elements (purple bars) are indicated. Red numbers indicate the Smith-Waterman (SW) alignment scores of these MIR elements. The SW alignment scores of MIRs in MIR-dependent human ciRS-7 (see Figure 1A) are 945 (upstream) and 1077 (downstream).

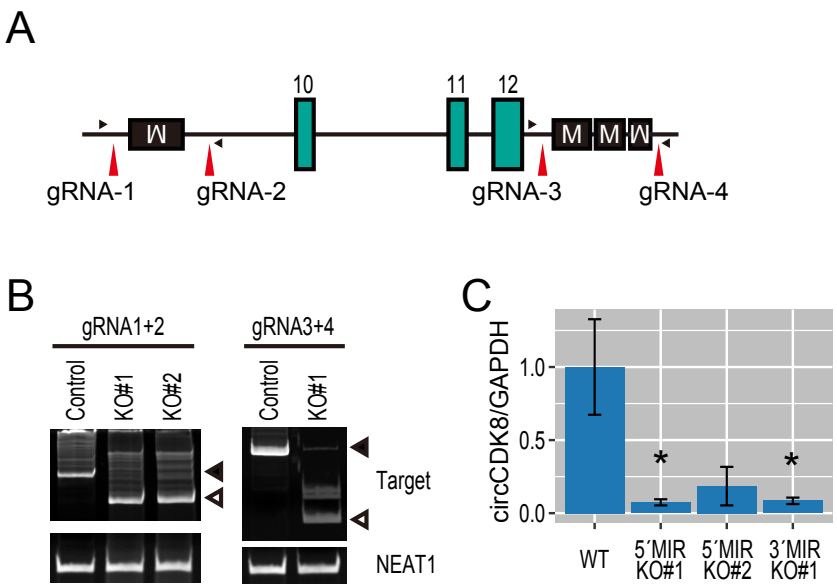

Figure S7. CRISPR/Cas9-Mediated Deletion of Either Upstream or Downstream MIRs Aborts the Production of circCDK8

(Related to Figure 3)

(A) Schematic genomic structure of circCDK8 locus with the flanking inverted MIR sequences. The positions of guide RNAs (gRNA1–gRNA4) to delete each MIR element are indicated with red vertical arrowheads. PCR primers for detecting deleted sites are indicated with filled triangles.

(B) The genomic deletions of the flanking MIR elements in HEK293 cells were verified by genomic PCR. The indicated two pairs of gRNAs were used to delete the 5′ and 3′ MIR elements. PCR primers indicated in panel A were used for detecting the MIR-deleted sites (open triangles in KO#1 and KO#2) and non-deleted sites (filled triangles in Control).

(C) The effects of the MIR deletions (5′MIR KO and 3′MIR KO) on the circCDK8 production was quantified by qRT–PCR. The ciRS-7 expression levels were normalized to the control expression level of GAPDH (circCDK8/GAPDH). Values are relative to the value of undeleted parental cells (WT). Means ± standard deviation (SD) are given for three independent experiments (*P < 0.05).

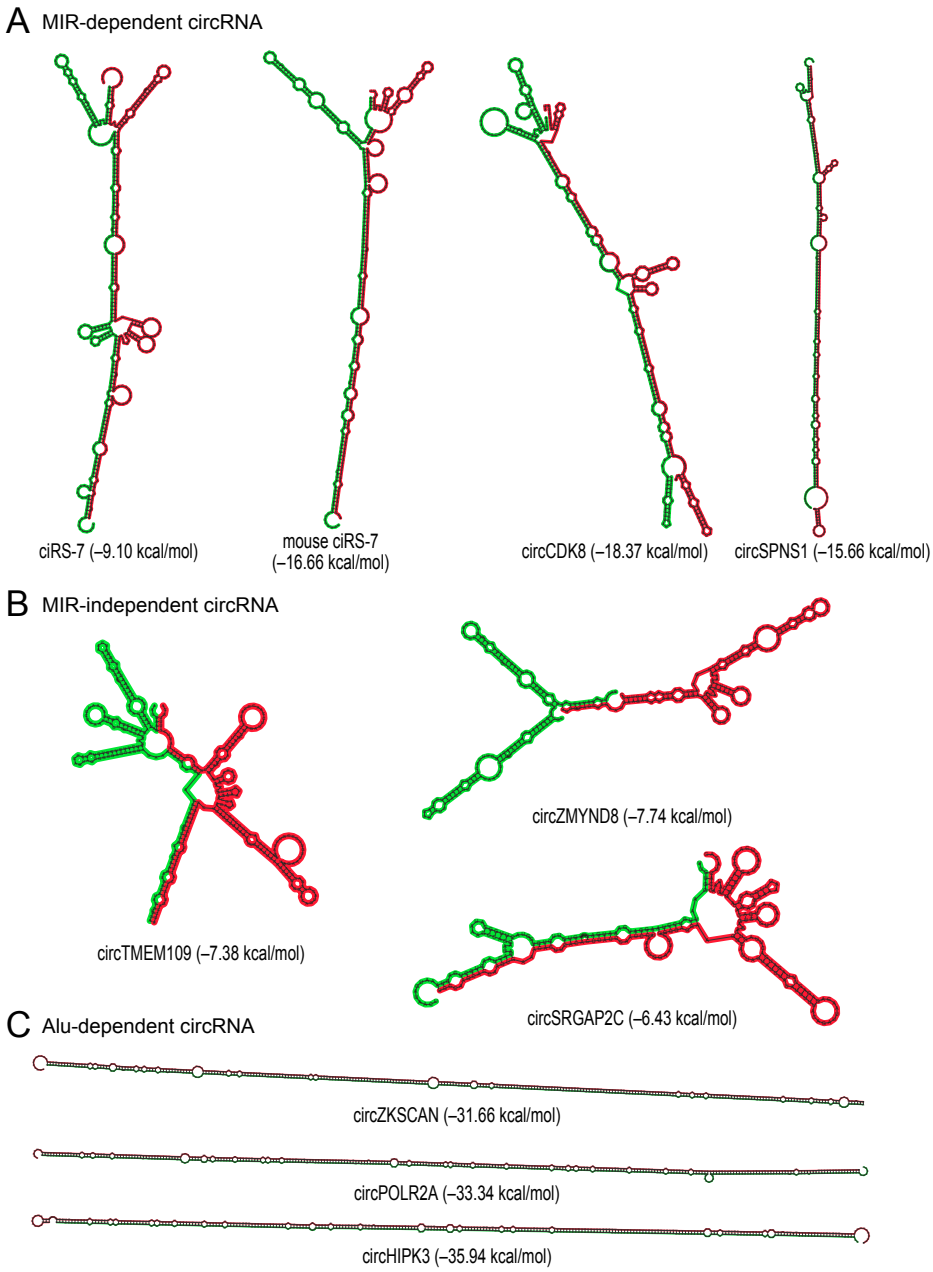

Figure S8. Inverted Sequences Are Less Complementary in MIRs than in *Alu*s
(Related to Figures 3–6)
RNA secondary structures were predicted by RNAcofold of the Vienna RNA package. The cofold structure of MIR-dependent circRNAs **(A)**, MIR-independent circRNAs (Cf. mouse ciRS-7, see Figure 1A) **(B)**, and *Alu*-dependent circRNAs **(C)** are shown. The corrected thermal stability (–kcal/mol) of each MIR was calculated by the RNAup program.

Table S1 List of all the synthetic oligonucleotides used in the experiments
(Related to Figures 1–3, 5, 6, S1, S3, S5, S7)

Primer DNAs for plasmids construction		
ciRS-7-5′/BamHI	5'-AAAGGATCCACCCCTGGGTTATTGGGTTGTGGAGAATCA-3'	For pcDNA3-ciRS-7
ciRS-7-3′/XhoI	5'-AAACTCGAGACCTTTGGATCACATCATTCTATCATGATT-3'	
ciRS-7-Δ5′MIR/BamHI	5'-AAAGGATCCATTATTATAACATGAATAAGCATTATGCAA-3'	For pcDNA3-ciRS-7ΔMIR
ciRS-7-Δ3′MIR/XhoI	5'-AAACTCGAGTCTTTGGTCATGTAAGACCAATGATAAAAA-3'	
circCDK8-5′/BamHI	5'-AAAGAATTCAATGCAGTCTCAGTCCAGCAG-3'	For pcDNA3-circCDK8
circCDK8-3′/XhoI	5'-TTTCTCGAGCACTCGGGACCTTATCAGTTT-3'	
ciRS-7-5′MIR-RC/BglII-F	5'-GAAGATCTACCCCTGGGTTATTGGGTT-3'	For pcDNA3-ciRS-7RC
ciRS-7-5′MIR-RC/BglII-R	5'-GAAGATCTGCAAACTCTCATATTCTGGTTG-3'	
circCDK8-Δ5′MIR-R	5'-ATCACACAGCTCTGTACTTTGTAAGTTGTG-3'	For pcDNA3-circCDK8Δ5′MIR
circCDK8-Δ5′MIR -F	5'-TCTGGGACTTGATGAAATGGCTTTTCTTCT-3'	
circCDK8-Δ3′MIR-R	5'-TGTCAGTACTTTTCCATGCCAGTAACATTT-3'	For pcDNA3-circCDK8Δ3′MIR
circCDK8-Δ3′MIR-F	5'-GCTATTGTTTTGGAACAATGTTTCACAGTG-3'	
circSPNS1-infusion-F	5'-TGACGATAAAGGATCCAGGGGTTGTCTTATTTAGA-3'	For pcDNA3-circSPNS1
circSPNS1-infusion-R	5'-TAGATGCATGCTCGACATCTATTAACTAATTTAATCCT-3'	
circSPNS1-Δ5′MIR-F	5'-TGACGATAAAGGATCTGGGAGCGGGCTGGTGAG-3'	For pcDNA3-circSPNS1ΔMIR
circSPNS1-Δ3′MIR-R	5'-TAGATGCATGCTCGAGACCCACGCCATCCCCCT-3'	
circTMEM109/BamHI	5'-AAAGGATCCGGAGACAATACAGCAGAGTTG-3'	For pcDNA3-circTMEM109
circTMEM109/XhoI	5'-TTTCTCGAGACATTGCAAAGGAATAAGCCG-3'	
circTMEM109-Δ5′MIR/BamHI	5'-AAAGGATCCTGAATGTTAGCTTTTTATTAA-3'	For pcDNA3-circTMEM109Δ5,3MIR
circTMEM109-Δ3′MIR/XhoI	5'-TTTCTCGAGTGGTGGCGGAAGTTCTTTTTT-3'	
circTMEM109-Δ5′MIR-F	5'-GTTATTCTTGTTTGAGCACATAACTGAGC-3'	
circTMEM109-Δ5′MIR-R	5'-AGGAGTCAAGTTATACTGTGGGTCT-3'	
circSRGAP2C/BamHI	5'-CCCAGATCTATCCAGAGGAGAGTCGGTGTT-3'	For pcDNA3-circSRGAP2C
circSRGAP2C/XhoI	5'-TTTCTCGAGATGTCAGGGGGAGCTGGATAC-3'	
circSRGAP2C-Δ5′MIR/BamHI	5'-CCCAGATCTCAATGTTTATTAAGTGGTAGA-3'	For pcDNA3-circSRGAP2CΔ5,3MIR
circSRGAP2C-Δ3′MIR/XhoI	5'-TTTCTCGAGGCATTGTAACTCTTTAGTTAA-3'	
circSRGAP2C-Δ5′MIR-F	5'-GGCATTGCAGTTGCTGTGA-3'	
circSRGAP2C-Δ5′MIR-R	5'-TCTAGACAACAACCCTATGAAGACTG-3'	
circSRGAP2C-Δ3′MIR-F	5'-AGCACCCTGATGGATCATGG-3'	
circSRGAP2C-Δ3′MIR-R	5'-TCGTCTATCTGCCAGGAAATACTTT-3'	
circZMYNDR8/BamHI	5'-CGGAATTCGGCCTAGACACAAAGGATCAAG-3'	For pcDNA3-circZMYNDR8
circZMYNDR8/XhoI	5'-TTTCTCGAGTGGAAAAGAAGCTGCTCAGAC-3'	
circZMYNDR8-Δ5′MIR/BamHI	5'-CCCAGATCTCAATGTTTATTAAGTGGTAGA-3'	For pcDNA3-circZMYNDR8Δ5,3MIR
circZMYNDR8-Δ3′MIR/XhoI	5'-TTTCTCGAGGGTCACATAACTTTTGATAGT-3'	
ciRS-7-5′MIR-R	5'-AGTCCATAAGCTTGGGTCTCC-3'	For pcDNA3-ciRS7-5MIR-51-241, pcDNA3-ciRS7-5MIR-101-241, and pcDNA3-ciRS7-5MIR-190-241
ciRS-7-5′MIR-F-51-241	5'-CAAATCCTGCCTCTACCAATTACCA-3'	
ciRS-7-5′MIR-F-101-241	5'-TAACCATTCCAGACTTCAGTTTCTG-3'	
ciRS-7-5′MIR-F-190-241	5'-AGATTATATGAAATGCTTAGTACAGTGCCT-3'	
ciRS-7-infusion-F	5'-TGCTGATGAGGGATACATGAAAC-3'	For pcDNA3-ciRS7-circCDK8MIR
ciRS-7-infusion-R	5'-CAAACTGCAGTACTGTTGGTTC-3'	
circCDK8MIR-infusion-F	5'-CAGTACTGCAGTTTGACTGGCATGGAAAAGTACTGAC-3'	
circCDK8MIR-infusion-R	5'-TATCCCTCATCAGCAAAAGTGGTACTGTGCAGTGC-3'	
circZMYNDR8MIR-infusion-F	5'-CAGTACTGCAGTTTGAGAATCCTACCTCGTACACTTACT-3'	For pcDNA3-ciRS7-circZMYNDR8MIR
circZMYNDR8MIR-infusion-R	5'-TATCCCTCATCAGCAACAGGACCTACCAACGGAGA-3'	
circHIPK3-infusion-F	5'-TGACGATAAAGGATCCACATTGAGAAGAATGGGAA-3'	For pcDNA3-ciRS7-circHIPK3Alu
circHIPK3-infusion-R	5'-TAGATGCATGCTCGACACGGGAGCCAAAGAAGT-3'	
circHIPK3Alu-infusion-F	5'-CAGTACTGCAGTTTGGTGTCATGTCAATGCCCAAAAAG-3'	
circHIPK3Alu-infusion-R	5'-TATCCCTCATCAGCAAACGGTGCCAACATTTTCCC-3'	
Primer DNAs for splicing products analysis		
ciRS-7-F(nested)	5'-TAAGGATGGCCCAGAAGGAG-3'	For PCR detection of alternatively spliced products from ciRS-7 precursor
ciRS-7-R(nested)	5'-GGAACAGTTAGGGATCCCTT-3'	
ciRS-7-F	5'-TCCGCGCCTTTGAGAGCTTTGGAACGATAT-3'	
ciRS-7-R	5'-CAGAAACAATGGCAATTATAATAGTTAAAC-3'	
circSPNS1-F(nested)	5'-TGCTCTTCCTCTGACAGTCTC-3'	For PCR detection of circSPNS1 cDNA
circSPNS1-R(nested)	5'-AAGAGGTCGGCAATGAGAGTG-3'	
circSPNS1-F	5'-GCGCGATGGTGGAATAACTG -3'	
circSPNS1-R	5'-TTCCTCTTCCTGTCCCTTGC -3'	

circCDK8-F	5'-TGAGAGTTGTTCCTCCTACCAC-3'	For PCR detection of circCDK8 cDNA
circCDK8-R	5'-TCCTGCATAGCCTGTTCTGAG-3'	
circTMEM109-F	5'-TTCTGTGGCCTTCTTTGCTC-3'	For PCR detection of circTMEM109 cDNA
circTMEM109-R	5'-AACACATGCTTTCCCCATGG-3'	
circZMYNDR8-F	5'-AGGAACCCAAAGAACCATCTCC-3'	For PCR detection of circZMYNDR8 cDNA
circZMYNDR8-R	5'-TTCTCAGAATCCTCCGAATCGC-3'	
circSRGAP2C-F	5'-CAACCAATGCATCTGTCTTCAAG-3'	For PCR detection of circSRGAP2C cDNA
circSRGAP2C-R	5'-GCTGTCGGCATTGTACATGTG-3'	
ciRS-7-F	5'-ACGTCTCCAGTGTGCTGA-3'	For PCR detection of ciRS-7 cDNA
ciRS-7-R	5'-CTTGACACAGGTGCCATC-3'	
GAPDH-F	5'-AGCCACATCGCTCAGACAC-3'	For PCR detection of GAPDH cDNA
GAPDH-R	5'-GCCCAATACGACCAAATCC-3'	
pcDNA3-3´UTR-F	5'-ATGCATCTAGAGGGCCCTATTC-3'	For PCR detection of circRNA precursor cDNAs from reporter pDNA3-plasmids
pcDNA3-3´UTR-R	5'-AACAACAGATGGCTGGCAAC-3'	
pcDNA5-FRT/TO 3´UTR-F	5'-AGTCTAGAGGGCCCGTTTAAAC-3'	For PCR detection of circRNA precursor cDNAs from reporter pDNA5-plasmids
pcDNA5-FRT/TO 3´UTR-R	5'-TTAGGAAAGGACAGTGGGAGTG-3'	
NEAT1-F	5'-AGTTGCATTCTCACCGTCAC-3'	For PCR detection of NEAT1 gene fragment (control)
NEAT1-R	5'-TGCCGATGAAGCAACAAAGC-3'	
ciRS-7-AS-gRNA1-2F	5'-ACTGACTTCTTGTCTGCTCTG G-3'	For PCR detection of ciRS-7 editing & un-editing by gRNA1/2
ciRS-7-AS-gRNA1-2R	5'-TGCCTGGATGTAGCAAATGC-3'	
ciRS-7-AS-gRNA2-3F	5'-TCCTAGATGGTGTGCTTCTCA C-3'	For PCR detection of ciRS-7 editing by gRNA2/3
ciRS-7-AS-gRNA2-3R	5'-CAGTCACACAGCTGGTAATTG G-3'	
ciRS-7-AS-gRNA2-3F'	5'-ATCGGGGGCACACAAGAATC-3'	For PCR detection of ciRS-7 un-editing by gRNA2/3
ciRS-7-AS-gRNA2-3R'	5'-TGCCATTGTCCTCAATCGTC-3'	
ciRS-7-AS-gRNA4-5F	5'-TTTCCTGCTCTGTAGAAAGTCA-3'	For PCR detection of ciRS-7 editing & un-editing by gRNA4/5
ciRS-7-AS-gRNA4-5R	5'-TCAGCTTGTCAGATGCCAGA-3'	
ciRS-7-5´MIR-gRNA1-2F	5'-CTACTTGGCAGTGGTATGGTGA-3'	For PCR detection of ciRS-7 editing & un-editing by gRNA1/2
ciRS-7-5´MIR-gRNA1-2R	5'-TGCAGATCAGGGAGTAACTTACAG-3'	
ciRS-7-3´MIR-gRNA3-4F	5'-ACTTCACTAGTGCTTACGGTTT-3'	For PCR detection of ciRS-7 editing & un-editing by gRNA3/4
ciRS-7-3´MIR-gRNA3-4R	5'-AAGCACCAGTACTCGAAGCA-3'	
circCDK8-5´MIR-gRNA1-2F	5'-TGGAAATGCAGGCTTTTGGC-3'	For PCR detection of circCDK8 editing & un-editing by gRNA1/2
circCDK8-5´MIR-gRNA1-2R	5'-GGGTCCATGGTAAGCAGCTT-3'	
circCDK8-3´MIR-gRNA3-4F	5'-GGGTTTATGATCGTGGGAAAATG-3'	For PCR detection of circCDK8 editing & un-editing by gRNA3/4
circCDK8-3´MIR-gRNA3-4R	5'-ACTGAACCCTTGTGTAGTTGGG-3'	
Antisense 2'-*O* -Me RNAs for blocking alternative splice sites (*:phosphothiorate backbone, mN: 2'-O-methyl oxyribonucleotides)		
GFP-ASO	5'-mG*mC*mA*mC*mC*mA*mU*mC*mU*mU*mC*mU*mU*mC*mA*mA*mG*mG*mA-3'	For off-target negative control
ciRS-7-ASO1	5'-mA*mU*mC*mG*mG*mA*mA*mA*mC*mC*mC*mU*mG*mG*mA*mC*mA*mU*mU*mG-3'	For 3´ splice site of ciRS-7
ciRS-7-ASO2	5'-mG*mU*mU*mA*mG*mA*mA*mU*mA*mC*mC*mU*mG*mG*mA*mU*mA*mU*mU*mG-3'	For 5' splice site of ciRS-7
ciRS-7-ASO3	5'-mA*mA*mA*mG*mG*mC*mU*mA*mA*mC*mC*mA*mG*mU*mU*mU*mU*mU*mG*mU-3'	For prox. Alt. 5' splice site of ciRS-7
ciRS-7-ASO4	5'-mU*mA*mC*mC*mA*mA*mU*mG*mU*mG*mC*mU*mA*mA*mA*mA*mG*mA*mA*mA-3'	For dist. Alt. 3' splice site of ciRS-7
ciRS-7-ASO5	5'-mG*mU*mC*mU*mU*mC*mU*mC*mA*mC*mA*mG*mG*mA*mG*mG*mU*mA*mG*mC-3'	For dist. Alt. 5' splice site of ciRS-7
ciRS-7-ASO6	5'-mA*mU*mC*mC*mA*mG*mA*mG*mA*mU*mC*mU*mA*mC*mA*mA*mA*mU*mU*mA-3'	For prox. Alt. 3' splice site of ciRS-7
Guide RNAs for editing alternative splice sites and MIR elements		
ciRS-7-AS-gRNA1	5'-TACTGTTGGTTCATAAGAT-3'	For positive control (gRNA1/2) & for deletion of alternative 5' splice site (gRNA2/3)
ciRS-7-AS-gRNA2	5'-CTCCACAACCCAATAACCCA-3'	
ciRS-7-AS-gRNA3	5'-AAGGTCAGGCTATCACGCTG-3'	
ciRS-7-AS-gRNA4	5'-TTTGAGCTAAATTGCCC-3'	For deletion of alternative 3' splice site (gRNA4/5)
ciRS-7-AS-gRNA5	5'-AACATCAATCTGCATTG-3'	
ciRS-7-MIR-gRNA1	5'-GTCCTGGCAGTACAACCCCT-3'	For deletion of ciRS-7 5´ MIR element (gRNA1/2+5´donor oligo)
ciRS-7-MIR-gRNA2	5'-AGGCGCAAACTCTCATATTC-3'	
ciRS-7-5´MIR-ODN	5'-CTTGTCTGCTCTGGGCTGGGGGCACCCTCTTTTTGGGTGAGTGGTGCTTAGTCCTGGCAGTACAACCCCT GATTTATTGGGTTATTATTATAACATGAATAAGCATTATGCAAATAGAATATGAGAGTTTGCGCCTATCTTTGCAAAATTT TCACACTTTGATACTTAATTTCCCTCAAATTAAGG-3'	
ciRS-7-MIR-gRNA3	5'-ATGATATTAATTTTTATCAT-3'	For deletion of ciRS-7 3´ MIR element (gRNA3/4+3´donor oligo)
ciRS-7-MIR-gRNA4	5'-ATGTGGAAGCAATCAACCTT-3'	
ciRS-7-3´MIR-ODN	5'-CTGGTATTTTAGGTAAAGTTAACATGTAGAGTATTATTTGTCCATTTTAAATGATATTAATTTTTATCATTATTC TTACATGACCAAAGAATAATAATAATATAATAATAATAATAATAATAATAACAACAACAACTGCTGTTTAAAATCATGATAG AATGATGTGATATAAAGGTTGATTGCTTCCACATTTTGTGTAGAATATTATACAATCCCGTATACAAATGGTCTCGCTTG ATCC-3'	
circCDK8-MIR-gRNA1	5'-TATACTCTGATCTAATGCAG-3'	For deletion of circCDK8 5´ MIR element (gRNA1/2)
circCDK8-MIR-gRNA2	5'-GTCAATCTCCCCATTACACC-3'	
circCDK8-MIR-gRNA3	5'-ATACTGACGTCTGTATACCC-3'	For deletion of circCDK8 3´ MIR element (gRNA3/4)
circCDK8-MIR-gRNA4	5'-CCATGATAGGATCCCTAAGC-3'	

TRANSPARENT METHODS

Analysis of RNA-Seq Datasets

We used RNA-Seq datasets from non-neoplastic brain tissue (GSE59612; Gill et al., 2014). Obtained data were aligned to reference human genome hg19 using HISAT2 (Kim et al., 2015) and the aligned sequence reads were assembled by StringTie (Pertea et al., 2015). Repeated sequences were downloaded from the RepeatMasker track in the UCSC table browser (https://genome.ucsc.edu/cgi-bin/hgTables) and analyzed with BEDtools (http://bedtools.readthedocs.io).

To search for potential MIR-dependent circRNAs, we used 'SupTable1-LOW_Backsplice_Set.xls' file (Supplemental Table S1 in Jeck et al., 2013) that contains the back-splice sites' information along with the chromosome location, the starting/ending positions in the chromosome, the corresponding strand, and the spliced reads per billion mapping (SRPBM) of identified 7771 circRNAs. The list of mouse circRNAs were obtained from circBase (Glažar et al., 2014) and the UCSC-LiftOver tool (https://genome.ucsc.edu/cgi-bin/hgLiftOver) was used to find mouse orthologous circRNAs.

The box plots were constructed using the R/Bioconductor package (http://www.bioconductor.org). For statistical comparisons of groups, Wilcoxon rank-sum tests were used to calculate P-values.

Possible RNA pairings between inverted MIRs were predicted using the RNAcofold program from the Vienna RNA package (Lorenz et al., 2011). Thermodynamic stability of the base-paired MIRs was calculated with the RNAup program in the Vienna RNA package using '–b' option to include the probability of unpaired regions (Lorenz et al., 2011). Exceptionally weak MIR-MIR base-pairings that the RNAup program could not calculate their thermodynamic stabilities were set to zero values ('All circRNAs' in Fig. 4D).

RT–PCR Assays

RT–PCR analysis was performed essentially as previously described (Yoshimoto et al., 2017). Human cerebral cortex total RNA was purchased from Clontech (CLN 636561). From culture cells, total RNA was isolated with a Nucleospin RNA kit (Machery Nagel) according to the manufacturer's instructions. 'On-column' DNase I digestion was performed to remove contaminated DNA. Purified RNA was reverse-transcribed using PrimeScript II (Takara Bio) with oligo-dT and random primers, and cDNA was amplified by PCR (20–30 cycles) with Ex-Taq (Takara Bio) and specific primers (Table S1). PCR-amplified products were analyzed by 8% polyacrylamide gel electrophoresis.

For nested PCR, the first PCR reaction mixture (30 cycles) was purified with a PCR cleanup column (Takara Bio) and the eluate was used for the second PCR reaction (30 cycles). The purified RNase R (1 μg) was added to digest 1 μg of total RNA to remove linear RNA in a 20 μL reaction mixture at 30ºC for 30 min as described previously (Suzuki et al., 2006).

To perform quantitative PCR (qPCR), a real-time PCR instrument (Eco Real-Time PCR System, Illumina) was used with the same primers (Table S1) that were used in the regular PCR. For the qPCR reactions, KAPA Taq PCR kit was used according to the manufacturer's protocol (Kapa Biosystems).

For the RT-qPCR analysis in Figure 2E, DNase-treated RNA (1 μg) was reverse-transcribed using a Superscript VILO cDNA Synthesis Kit (Thermo Fisher Scientific) according to the manufacturer's instructions. Obtained cDNA was mixed with SYBR Green I Master (Roche Molecular Systems) and analyzed on a real-time PCR instrument (LightCycler 480, Roche Molecular Systems) according to the manufacturer's protocol.

Northern Blot Analyses

Total RNAs (5 μg each) were separated by electrophoresis on 1% agarose containing 3% formaldehyde, rinsed twice in distilled water for 10 min, denatured in 7.5 mM NaOH for 20 min, neutralized in 20× SSC containing 3 M NaCl and 0.3 M sodium citrate (pH 7.0) for 20 min, and blotted overnight on a nylon membrane (RPN82B, GE Healthcare Life Sciences) followed by UV irradiation at 254 nm with 120 mJ/cm^2 (CL-1000, Funakoshi). DIG-labeled probes were

hybridized in PerfectHyb solution (HYB-101, Toyobo) overnight at 68ºC, and hybridized probes were detected by alkaline phosphatase-conjugated anti-DIG antibodies (#11093274910, Roche) and CDP-star (#CDP-RO, Roche). The chemiluminescence signals were observed by imaging analyzer (ImageQuant LAS 500, GE Healthcare Life Sciences).

Antisense Oligoribonucleotide-Mediated Splicing Repression

Antisense 2′-*O*-methyl-modified phosphorothioate oligoribonucleotides (ASOs) were purchased from Integrated DNA Technologies (Table S1). These chemically modified ASOs were electroporated into SH-SY5Y cells (Gene Pulser Xcell, Bio-Rad). Fully confluent SH-SY5Y cells grown on 10 cm plate in D-MEM/Ham's-F12 medium (Fujifilm Wako) were trypsinized and the washed cell pellets were suspended in 1 mL OPTI-MEM medium (Thermo Fisher Scientific). This cell suspension (0.2 mL) plus ASO (2.5–10 μM final concentration) were transferred into 0.4 cm cuvette (BEX) and electroporated at 200 V for 20 ms square-wave pulses. After electroporation, cell suspensions were transferred into 6-well plates supplemented with 1.8 mL D-MEM/Ham's-F12 that was cultured for 24 h before RT–PCR analysis.

Construction and Expression of circRNA-Reporter Plasmids

The expression plasmids for ciRS-7, circCDK8, circTMEM109, circZMYNDR8, and circSRGAP2C were constructed by subcloning the PCR-amplified fragments into FLAG-pcDNA3 vector using BamHI and XhoI sites (Yoshimoto et al., 2009). The expression plasmids for circSPNS1 and circHIPK3 were constructed by subcloning the PCR-amplified fragments into FLAG-pcDNA3 plasmid using an In-Fusion HD cloning kit (Takara Bio) according to the manufacturer's protocol. The deletion of MIR element (Δ5′MIR, Δ3′MIR, Δ5′3′MIR) of these expression plasmids were made by KOD -Plus- Mutagenesis Kit (TOYOBO) according to the manufacturer's protocol. The expression plasmid for ciRS-7-5′MIR-RC was constructed by subcloning the PCR-amplified 5′MIR fragment into pcDNA3-ciRS-7Δ5′MIR vector using BglII and BamHI sites. The expression plasmids for ciRS-7 with flanking repeat elements derived from either circCDK8, circZMYND8, or circHIPK3, were constructed by subcloning the PCR-amplified ciRS-7 fragment into pcDNA3-circCDK8, pcDNA3-circZMYNDR8, or pcDNA3-circHIPK3 plasmids, respectively, using an In-Fusion HD cloning kit.

To establish HEK293 cells stably expressing ciRS-7, PCR-amplified a ciRS-7 fragment was subcloned into pcDNA5 FRT-TO vector (Thermo Fisher Scientific) using BamHI and XhoI sites, and transfected into Flp-In T-REx 293 cells (Thermo Fisher Scientific) along with Flp recombinase vector pOG44. The transfected cells were treated with 1 μg/mL DOX for 24 h and total RNA was prepared for the RT–PCR analysis. To inhibit the splicing reaction, 100 ng/mL SSA was added 18 h after DOX treatment.

Mouse N2A cells were transiently transfected with these expression plasmids using Lipofectamine 2000 (Thermo Fischer Scientific) according to the manufacturer's instructions. The transfected cells were incubated for 24 h and total RNA was prepared for RT–PCR analysis.

Targeted Genomic Deletion of the Splice Sites in the ciRS-7 Locus and of MIRs in the circCDK8 Locus

Cas9 RNP was introduced with the Alt-R CRISPR-Cas9 System (Integrated DNA Technologies) according to the manufacturer's instructions. The gRNAs in Figures S3A and S7A and primer sequences are listed in Table S1.

HEK293 cells were seeded into a 96-well plate at a density of 4×10^4 cells/well with DMEM/F-12 medium (Fujifilm Wako Pure Chemical) containing 10% fetal bovine serum (FBS, Sigma-Aldrich) and 0.5% Gibco penicillin-streptomycin mixture (Thermo Fisher Scientific). The cells were transiently transfected with 0.75 pmol of Cas9 RNP using 1.2 μL of Lipofectamine RNAiMAX (Life Technologies) diluted up to 50 μL of OPTI-MEM (Thermo Fisher Scientific). After a 20 min incubation at room temperature, the transfection solution was added dropwise to the cells. At 48 h post-transfection, the cells were trypsinized and filtered through a 40 μm

Corning cell strainer (Thermo Fisher Scientific), seeded onto a 10-cm culture plate, and grown for 2 weeks. Each colony (~96 clones per construct) were picked, trypsinized, and seeded onto 96-well plate with two replicates. Genomic DNA was extracted and PCR was performed to verify the deleted region.

Targeted Genomic Deletion of MIRs in ciRS-7 Locus

The gRNAs (Figure 2C) are listed in Table S1. The annealed gRNAs were subcloned into the BpiI-cleaved (Thermo Fisher Scientific) site of a modified version of CRSPR vector px458 (#43138, Addgene) without the ITR element that expresses Cas9/EGFP (Højland Knudsen et al., 2018). To increase the efficiency and accuracy of the CRISPR targeting site (MIR elements), single-stranded donor oligodeoxyribonucleotides (ssODN) acting as repair templates were used (Table S1).

SH-SY5Y cells were seeded in six-well plates and grown to 70% confluency (0.8×10^6 cells/well) in DMEM/F-12 medium containing GlutaMax, 10% FBS, and 0.5% Gibco penicillin-streptomycin mixture (all reagents from Thermo Fisher Scientific). The cells were transiently transfected with 2.5 µg DNA (1 µg each of two gRNA vectors and 0.5 µg ssODN) using Lipofectamine 3000 (Thermo Fisher Scientific) according to the manufacturer's instructions. After 15 min incubation at room temperature, the transfection solution was added dropwise to the cells. The medium was replaced with fresh growth medium at 12 h post-transfection.

At 48 h post-transfection, the cells were prepared for fluorescent-activated cell sorting (FACS) by trypsinization, washing, and re-suspension in PBS with 2% FBS. The cells were FACS sorted in a BD FACSAria III (BD Biosciences) based on their viability and GFP signal quality into 96-well plates (single cell per well) containing 150 µl of conditioned growth medium (30% used and 70% fresh media). Three weeks after the FACS sorting, the grown colonies were passaged into duplicate 96-well plates and one set was used for DNA preparation and genomic PCR with flanking primers to detect the deleted homozygote clones. The verified deleted genomic clones and the appropriate controls were expanded and total RNA was prepared for RT-qPCR analysis (see above).

SUPPLEMENTAL REFERENCES

Gill, B.J., Pisapia, D.J., Malone, H.R., Goldstein, H., Lei, L., Sonabend, A., Yun, J., Samanamud, J., Sims, J.S., Banu, M.*, et al.* (2014). MRI-localized biopsies reveal subtype-specific differences in molecular and cellular composition at the margins of glioblastoma. Proc. Natl. Acad. Sci. USA *111*, 12550–12555.

Glažar, P., Papavasileiou, P., and Rajewsky, N. (2014). circBase: a database for circular RNAs. RNA *20*, 1666–1670.

Højland Knudsen, C., Ásgrímsdóttir, E.S., Rahimi, K., Gill, K.P., Frandsen, S., Hvolbøl Buchholdt, S., Chen, M., Kjems, J., Febbraro, F., and Denham, M. (2018). A Modified Monomeric Red Fluorescent Protein Reporter for Assessing CRISPR Activity. Front. Cell Dev. Biol. *6*, 54.

Jeck, W.R., Sorrentino, J.A., Wang, K., Slevin, M.K., Burd, C.E., Liu, J., Marzluff, W.F., and Sharpless, N.E. (2013). Circular RNAs are abundant, conserved, and associated with ALU repeats. RNA *19*, 141–157.

Kim, D., Langmead, B., and Salzberg, S.L. (2015). HISAT: a fast spliced aligner with low memory requirements. Nat. Methods *12*, 357–360.

Lorenz, R., Bernhart, S.H., Honer Zu Siederdissen, C., Tafer, H., Flamm, C., Stadler, P.F., and Hofacker, I.L. (2011). ViennaRNA Package 2.0. Algorithms. Mol. Biol. *6*, 26.

Pertea, M., Pertea, G.M., Antonescu, C.M., Chang, T.C., Mendell, J.T., and Salzberg, S.L. (2015). StringTie enables improved reconstruction of a transcriptome from RNA-seq reads. Nat. Biotechnol. *33*, 290–295.

Suzuki, H., Zuo, Y., Wang, J., Zhang, M.Q., Malhotra, A., and Mayeda, A. (2006). Characterization of RNase R-digested cellular RNA source that consists of lariat and circular RNAs from pre-mRNA splicing. Nucleic Acids Res. *34*, e63.

Yoshimoto, R., Kaida, D., Furuno, M., Burroughs, A.M., Noma, S., Suzuki, H., Kawamura, Y., Hayashizaki, Y., Mayeda, A., and Yoshida, M. (2017). Global analysis of pre-mRNA subcellular localization following splicing inhibition by spliceostatin A. RNA *23*, 47–57.

Yoshimoto, R., Kataoka, N., Okawa, K., and Ohno, M. (2009). Isolation and characterization of post-splicing lariat-intron complexes. Nucleic Acids Res. *37*, 891–902.